The Canadian Mineralogist
Vol. 52, pp. 351-371 (2014)
DOI: 10.3749/canmin.52.2.351

THE STABILITY OF Fe-RICH ALLUAUDITES IN GRANITIC PEGMATITES: AN EXPERIMENTAL INVESTIGATION OF THE Na–Fe^{2+}–Fe^{3+} (+PO_4) SYSTEM

FRÉDÉRIC HATERT[§], MAXIME BAIJOT, AND FABRICE DAL BO

Laboratoire de Minéralogie, B18, Université de Liège, B-4000 Liège, Belgium

ABSTRACT

In order to assess the stability of Fe-rich alluaudites in pegmatites, we performed hydrothermal experiments between 400 and 700 °C (1 kbar), in the Na–Fe^{2+}–Fe^{3+} (+PO_4) ternary system. These experiments produced several new phosphate minerals, among which was $Na_2Fe^{3+}(HPO_4)(PO_4)\cdot H_2O$ [*a* 15.5004(8), *b* 7.1465(5), *c* 29.239(2)Å, *V* 3238.9(3)Å^3, *Pnma*], which shows a crystal structure based on chains of corner-sharing FeO_6 octahedra, similar to those occurring in the jahnsite-group minerals. Alluaudite-type phosphate minerals occupy a large stability field in the center of the Na–Fe^{2+}–Fe^{3+} (+PO_4) system; this stability field covers between 5.8 (500 °C) and 21.1% (700 °C) of the diagram surface. A comparison of the chemical composition of natural Fe-rich alluaudite-type phosphate minerals with the experimental data obtained herein indicates that these minerals crystallized below *ca*. 450 °C in pegmatites. This temperature value is in good agreement with the secondary Na-metasomatic origin of these phosphate minerals. Moreover, a structural classification of phosphates occurring in the Na–Fe^{2+}–Fe^{3+} (+PO_4) diagram has been established, taking into account the connectivity between FeO_6 octahedra occurring in the crystal structures of the synthesized phases. This classification indicates a variation of the structural complexity of phosphates, characterized by an increasing dilution of FeO_6 octahedra in the structure as the Na content increases.

Keywords: Fe-rich alluaudites, Na–Fe^{2+}–Fe^{3+} phosphates, granitic pegmatites, phase relations, geothermometry, structural complexity

INTRODUCTION

In rare-element pegmatites of the beryl-columbite-phosphate and spodumene subtypes (Černý 1991, Černý & Ercit 2005), Fe-Mn phosphate minerals occur as nodules enclosed in silicate minerals; these nodules can reach several meters in diameter (Simmons *et al*. 2003). Among the Fe-Mn phosphates, minerals of the triphylite-lithiophilite series, $LiFe^{2+}(PO_4)$–$LiMn(PO_4)$, are the most common primary phases. Minerals of the alluaudite group, with ideal compositions ranging from $Na_2Mn(Fe^{2+}Fe^{3+})(PO_4)_3$ to $\square NaMnFe^{3+}_2(PO_4)_3$, are generally produced from primary triphylite-lithiophilite, by oxidation coupled with a Li → Na metasomatic exchange process. The existence of primary alluaudites, first mentioned by Quensel (1957), was confirmed by Fransolet *et al*. (1998, 2004), who observed several assemblages involving primary alluaudites: alluaudite + arrojadite at Hagendorf-Süd, Germany; alluaudite + fillowite at Rusororo, Rwanda, and Kabira, Uganda; and alluaudite + ferrisicklerite + heterosite at Kibingo and Wasurenge, Rwanda.

As observed for the phosphates of the triphylite-lithiophilite series, which progressively transform to ferrisicklerite-sicklerite, $Li_{1-x}(Fe^{3+},Mn^{2+})(PO_4)$–$Li_{1-x}(Mn^{2+},Fe^{3+})(PO_4)$, and to heterosite-purpurite, $(Fe^{3+},Mn^{3+})(PO_4)$–$(Mn^{3+},Fe^{3+})(PO_4)$, due to oxidation and Li-leaching, the primary alluaudites, which are weakly oxidized, progressively transform into oxidized secondary alluaudites. In order to maintain charge balance, Na is leached out of the alluaudite structure, according to the substitution mechanism $Na^+ + Fe^{2+} \rightarrow \square + Fe^{3+}$, as observed by Mason (1941) and Fransolet *et al*. (1985, 1986, 2004). This oxidation mechanism, coupled with Na-leaching, explains the transformation of hagendorfite, $Na_2MnFe^{2+}Fe^{3+}(PO_4)_3$, into alluaudite, $\square NaMnFe^{3+}_2(PO_4)_3$, and of ferrohagendorfite, $Na_2Fe^{2+}_2Fe^{3+}(PO_4)_3$, into ferroalluaudite, $\square NaFe^{2+}Fe^{3+}_2(PO_4)_3$.

In order to confirm the existence of primary alluaudites, Hatert *et al*. (2006) investigated the $Na_2(Mn_{1-x}Fe^{2+}_x)_2Fe^{3+}(PO_4)_3$ series (x = 0 to 1), which reflects the compositions of natural, weakly oxidized, primary alluaudites. The authors showed that, when the oxygen

§ *Corresponding author e-mail address*: fhatert@ulg.ac.be

fugacity is controlled by the Ni-NiO buffer, single-phase alluaudites crystallize at 400 and 500 °C, whereas the association alluaudite + marićite appears between 500 and 700 °C. The limit between these two fields corresponds to the maximum temperature that can be reached by alluaudites in granitic pegmatites, because marićite has never been observed in these geological environments.

Hatert *et al.* (2011) synthesized alluaudite + triphylite assemblages, similar to those observed in the Buranga, Kibingo (Rwanda), and Hagendorf-Süd (Germany) pegmatites. These authors detected significant amounts of Na in high-temperature triphylite; the Na-in-triphylite geothermometer indicates a crystallization temperature above *ca.* 420 °C for alluaudite from the Angarf-Sud pegmatite, Morocco.

Since alluaudites contain Na, Mn^{2+}, Fe^{2+}, and Fe^{3+} as dominant cations, the determination of the stability fields of alluaudite-type phosphates would require a complete investigation of the Na–Mn–Fe^{2+}–Fe^{3+} (+PO_4) quaternary system. Due to the crystal-chemical complexity of alluaudites, the investigation of this quaternary system is extremely difficult; for this reason, we decided first to explore the stability of Fe-rich alluaudites in the Mn-free Na–Fe^{2+}-Fe^{3+} (+PO_4) ternary system. The aim of this paper is to report on the results of these experiments, which will provide a tool for constraining the temperature that prevailed in pegmatites during the crystallization of Fe-rich alluaudite-bearing phosphate assemblages.

Experimental Procedure

The hydrothermal experiments were performed between 400 and 700 °C at 1 kbar, starting from several compositions distributed on the surface of the Na–Fe^{2+}–Fe^{3+} (+PO_4) ternary system. These starting compositions are reported in Table 1, along with the synthesis temperatures and the synthesized compounds. Stoichiometric quantities of $NaH_2PO_4{\cdot}H_2O$ (Merck, Darmstadt, Germany, min. 99 %), $Na_2HPO_4{\cdot}2H_2O$ (Merck, Darmstadt, Germany, min. 99.5 %), FeO (Aldrich, Steinheim, Germany, 99 %), Fe_2O_3 (Acros, Geel, Belgium, 99.999 %), Fe (Merck, Darmstadt, Germany, min. 99.5 %), $FePO_4$, Na_3PO_4, and $Na_3Fe^{3+}{}_2(PO_4)_3$ were homogenized in a mortar, under acetone in order to prevent oxidation

TABLE 1. RESULTS OF HYDROTHERMAL EXPERIMENTS PERFORMED IN THE Na–Fe^{2+}–Fe^{3+} (+PO_4) SYSTEM

Starting compositions	*T* (°C)	*P* (kbar)	fO_2	Duration (days)	Experimental products	Experiment no.
$Na_3(PO_4)$	400	1	-	3	α-, β-, and γ-Na_3PO_4 + $Na_2H_2P_2O_7{\bullet}6H_2O$	H.220
	500	1	-	3	α-, β-, and γ-Na_3PO_4 + $Na_2H_2P_2O_7{\bullet}6H_2O$	H.229
	600	1	-	3	α-, β-, and γ-Na_3PO_4 + $Na_2H_2P_2O_7{\bullet}6H_2O$	H.230
	700	1	-	3	$Na_2(HPO_4){\bullet}7H_2O$	H.286
$Fe^{3+}(PO_4)$	400	1	-	3	$Fe^{3+}{}_4(PO_4)_3(OH)_3$ + $Fe^{3+}{}_4(P_2O_7)_3$	H.221
	500	1	-	4	$Fe^{3+}{}_4(PO_4)_3(OH)_3$ + $Fe^{2+}{}_3Fe^{3+}{}_4(PO_4)_6$ + $Fe^{3+}{}_4(P_2O_7)_3$?	H.271
	600	1	-	4	$Fe^{3+}{}_4(PO_4)_3(OH)_3$ + $Fe^{3+}{}_4(P_2O_7)_3$ + $Fe^{2+}{}_3Fe^{3+}{}_4(PO_4)_6$ (tr.) + ?	H.272
	700	1	-	3	$Fe^{3+}{}_4(PO_4)_3(OH)_3$ + $Fe^{2+}{}_3Fe^{3+}{}_4(PO_4)_6$ + $Fe^{3+}{}_4(P_2O_7)_3$ + $Fe^{2+}{}_2P_2O_7$	H.282
$Fe^{2+}{}_3(PO_4)_2$	400	1	-	3	Sarcopside + $Fe^{2+}{}_3Fe^{3+}{}_4(PO_4)_6$ + magnetite (tr.) + iron (tr.)	H.228
	500	1	-	3	Sarcopside + $Fe^{2+}{}_3Fe^{3+}{}_4(PO_4)_6$ + iron (tr.) + magnetite (tr.)	H.247
	600	1	-	3	Sarcopside + $Fe^{2+}{}_3Fe^{3+}{}_4(PO_4)_6$ (tr.) + iron (tr.) + magnetite (tr.)	H.248
	700	1	-	3	Sarcopside	H.281
$NaFe^{2+}(PO_4)$	400	1	-	3	Marićite + Fe (tr.)	H.217
	500	1	-	3	Marićite + alluaudite (tr.)?	H.218
	600	1	-	3	Marićite + alluaudite	H.219
$Na_3Fe^{3+}{}_2(PO_4)_3$	400	1	-	3	Alluaudite	H.222
	700	1	-	3	Alluaudite + marićite + $NaH_2PO_4{\bullet}nH_2O$?	H.287
	700	1	HM	7	Alluaudite	H.317
$Na_{2.25}Fe^{3+}{}_{2.25}(PO_4)_3$	400	1	-	3	Alluaudite + ? (tr.)	H.265
	700	1	-	3	Alluaudite + marićite + X-phase	H.283
	700	1	HM	7	Alluaudite	H.318
$NaFe^{3+}{}_{2.6667}(PO_4)_3$	700	1	HM	7	Alluaudite	H.315
$NaFe^{2+}{}_4(PO_4)_3$	400	1	-	4	Sarcopside + alluaudite + marićite (tr.) + FeO (tr.)	H.268
	500	1	-	4	Sarcopside + alluaudite + magnetite (tr.) + iron (tr.) + marićite (tr.) ?	H.269
	600	1	-	4	Alluaudite + sarcopside + iron (tr.) + marićite (tr.) ?	H.270
	700	1	-	3	Alluaudite + sarcopside + $Fe_3(PO_4)_2{\bullet}nH_2O$ + hematite (tr.)	H.278
$Na_2Fe^{2+}{}_2Fe^{3+}(PO_4)_3$	400	1	-	3	Alluaudite + magnetite (tr.) + FeO (tr.)	H.223
	500	1	-	3	Alluaudite + marićite (tr.) + magnetite (tr.)	H.257
	600	1	-	3	Alluaudite + marićite (tr.)	H.258

TABLE 1. CONTINUED

Starting compositions	T (°C)	P (kbar)	fO_2	Duration (days)	Experimental products	Experiment no.
$Na_{1.5}Fe^{2+}_{1.5}Fe^{3+}_{1.5}(PO_4)_3$	400	1	-	3	Alluaudite + $Fe^{3+}_4(PO_4)_3(OH)_3$ (tr.) + FeO (tr.) + Fe (tr.)	H.224
$NaFe^{2+}Fe^{3+}_2(PO_4)_3$	400	1	-	3	Alluaudite + $Fe^{3+}_4(PO_4)_3(OH)_3$ + $Fe^{2+}_3Fe^{3+}_4(PO_4)_6$ + magnetite (tr.)	H.227
	500	1	-	3	Alluaudite + $Fe^{3+}_4(PO_4)_3(OH)_3$ + $NaFe^{3+}(P_2O_7)$ + $Fe_7(PO_4)_6$	H.255
	500	1	*	3	Alluaudite + $Fe_2P_2O_7$ + magnetite (tr.)	H.253
	600	1	-	3	Alluaudite + $NaFe^{3+}(P_2O_7)$ + $Fe_7(PO_4)_6$	H.256
	600	1	*	3	Alluaudite + $Fe_2P_2O_7$	H.254
	700	1	-	3	Alluaudite + $Fe_2P_2O_7$	H.279
	700	1	*	3	Alluaudite + $Fe_2P_2O_7$	H.280
	700	1	HM	7	Alluaudite	H.316
$Na_{1.895}Fe^{2+}_{1.421}Fe^{3+}_{1.421}(PO_4)_3$	400	1	-	3	Alluaudite + $NaFe^{3+}(P_2O_7)$ (tr.) + FeO (tr.)	H.241
$Na_{1.8}Fe^{2+}_{0.9}Fe^{3+}_{1.8}(PO_4)_3$	400	1	-	3	Alluaudite + $NaFe^{3+}(P_2O_7)$ + FeO (tr.)	H.242
	500	1	-	3	Alluaudite + $NaFe^{3+}(P_2O_7)$ + magnetite (tr.) + hematite (tr.)	H.259
	600	1	-	3	Alluaudite + $NaFe^{3+}(P_2O_7)$ (tr.) + magnetite (tr.) + hematite (tr.)	H.260
	700	1	-	3	Alluaudite + $Fe_2P_2O_7$	H.284
$Na_4Fe^{2+}Fe^{3+}(PO_4)_3$	400	1	-	3	$Na_7Fe^{2+}Fe^{3+}_3(PO_4)_6$ + marićite + $Na_2HPO_4 \bullet nH_2O$ + $Na_{4-2x}Fe^{3+}(PO_4)_{2-x}(HPO_4)_x(OH)_{1-x} \bullet xH_2O$ + iron (tr.) + FeO (tr.)	H.263
	500	1	-	3	Marićite + $Na_4Fe^{2+}Fe^{3+}(PO_4)_3$ + $Na_7Fe^{2+}Fe^{3+}_3(PO_4)_6$ + iron (tr.) + magnetite (tr.)	H.261
	600	1	-	3	$Na_4Fe^{2+}Fe^{3+}(PO_4)_3$ + marićite + $Na_3Fe^{3+}(PO_4)_2$ + $Na_2HPO_4 \bullet nH_2O$ (tr.) + $Na_{4-2x}Fe^{3+}(PO_4)_{2-x}(HPO_4)_x(OH)_{1-x} \bullet xH_2O$ + magnetite (tr.)	H.262
	700	1	-	3	Marićite + $Na_3Fe^{3+}(PO_4)_2$ + $Na_2HPO_4 \bullet nH_2O$ + magnetite (tr.)	H.285
$Na_{2.5}Fe^{2+}_{2.5}Fe^{3+}_{0.5}(PO_4)_3$	400	1	-	3	Alluaudite + marićite + $Na_2HPO_4 \bullet nH_2O$ (tr.) + FeO (tr.)	H.264
	500	1	-	4	Marićite + alluaudite + magnetite (tr.)	H.273
	600	1	-	4	Marićite + alluaudite	H.274
	700	1	-	3	Marićite + alluaudite	H.277

*: AgPd tubes

of FeO and Fe. $FePO_4$, Na_3PO_4, and $Na_3Fe^{3+}_2(PO_4)_3$ were previously synthesized by solid-state reactions in air, starting from stoichiometric mixtures of $NH_4H_2PO_4$ (Merck, min. 99 %) and $FeSO_4 \cdot 7H_2O$ (Merck, min. 99.5 %) (for $FePO_4$, T = 950 °C, duration = 3 days), $NaHCO_3$ (Merck, Darmstadt, Germany, min. 99.5%) and $NH_4H_2PO_4$ (for Na_3PO_4, T = 900 °C, duration = 18h), $NaHCO_3$, Fe_2O_3, and $NH_4H_2PO_4$ [for $Na_3Fe^{3+}_2(PO_4)_3$, T = 900 °C, duration = 1 day], which were heated in a platinum crucible.

Approximately 20 to 30 mg of the starting material was welded, together with 2 µl of distilled water, into small gold tubes with an outer diameter of 2 mm, a wall thickness of 0.1 mm, and a length of 25 mm. A few experiments were performed under a high O fugacity corresponding to that of the hematite-magnetite buffer (HM; Table 1); the oxygen fugacity was then controlled by using a double-capsule device similar to that developed by Eugster (1957). In these experiments, the samples were sealed into $Ag_{70}Pd_{30}$ tubes, identical in size to the small gold tubes described previously. Approximately 100 to 300 mg of a Fe_2O_3 + Fe_3O_4 homogeneous mixture (HM oxygen fugacity buffer, Norton 1955) were introduced, together with 10 µl of distilled water, into large gold tubes of 4 mm outer diameter, 0.1 mm wall thickness, and 40 mm length. The $Ag_{70}Pd_{30}$ tubes were then placed in the larger gold tubes which were also welded. The gold capsules were finally introduced into a conventional hydrothermal apparatus with vertically arranged Tuttle-type cold-seal

bombs (Tuttle 1949) for 3 to 7 days and then cooled in a stream of cold air. Pressure and temperature errors are estimated to be within ±3% and ±10 °C, respectively. After the experiment, the buffer was examined by X-ray powder diffraction, in order to check if the mixture was still present.

The powder X-ray diffraction patterns of the synthesized compounds were recorded with a Philips PW-3710 diffractometer using 1.9373 Å Fe$K\alpha$ radiation. The unit-cell parameters were calculated with the LCLSQ 8.4 least-squares refinement program (Burnham 1991) from the *d*-spacings calibrated with $Pb(NO_3)_2$ as an internal standard.

Electron-microprobe analyses were performed with Cameca SX-50 instruments located in Bochum, Germany (analyst H.-J. Bernhardt), and in Toulouse, France (analyst P. de Parseval), which operated in the wavelength-dispersion mode. Accelerating voltage and beam current were 15 kV / 15 nA in Bochum and 15 kV / 20 nA in Toulouse. The standards used in Bochum were graftonite from Kabira (sample KF16, Fransolet 1975) (for Fe, P), and jadeite (Na); those used in Toulouse were graftonite from Sidi-bou-Othmane (P), hematite (Fe), and albite (Na).

The X-ray structural study of $Na_4Fe^{3+}(PO_4)_2(OH)$ was carried out with an Agilent Technologies Excalibur 4-circle diffractometer equipped with an EOS CCD-area detector, on a crystal fragment measuring 0.11 × 0.13 × 0.27 mm. A total of 172 frames with a spatial resolution of 1° were collected by the ϕ/ω scan technique, with a counting time of 37 s per frame, in the range $5.86 < 2\theta < 52.65°$. A total of 10232 reflections were extracted from these frames, corresponding to 3570 unique reflections. Data were corrected for Lorenz, polarization, and absorption effects, the latter with an empirical method using the SCALE3 ABSPACK scaling algorithm included in the CrysAlisRED package (Oxford Diffraction 2007).

Phase Characterization

Alluaudite-type phosphates

The crystal structure of alluaudite [*a* 12.004(2), *b* 12.533(4), *c* 6.404(1) Å, β 114.4(1)°, *C*2/*c*] consists of kinked chains of edge-sharing octahedra stacked parallel to {101}. These chains are formed by a succession of *M*(2) octahedral pairs linked by highly distorted *M*(1) octahedra. Equivalent chains are connected in the *b* direction by the P(1) and P(2) phosphate tetrahedra to form sheets oriented perpendicular to [010]. These interconnected sheets produce channels parallel to *c* that contain the distorted cubic *A*(1) site and the *A*(2)' site, which exhibits a morphology of gable disphenoid. The general structural formula of alluaudite-type phosphates is $[A(2)A(2)'A(2)''_2][A(1)A(1)'A(1)''_2]M(1)M(2)_2(PO_4)_3$ (Hatert *et al.* 2000, 2003, 2005, Hatert 2008, Rondeux & Hatert 2010, Krivovichev *et al.* 2013); in natural alluaudites, the large crystallographic *A* sites are occupied by Na^+, Ca^{2+}, or Mn^{2+}, and the distorted octahedral *M* sites are occupied by Mn^{2+}, Fe^{2+}, Fe^{3+}, Al^{3+}, or Mg^{2+} (Moore & Ito 1979).

Alluaudite-type phosphates have been obtained from all experiments located in the central portion of the Na–Fe^{2+}–Fe^{3+} (+ PO_4) ternary system. They are frequently associated with maricite or sarcopside when the starting composition is rich in Fe^{2+}, and with $Fe^{3+}{}_4(PO_4)_3(OH)_3$ or $NaFe^{3+}(P_2O_7)$ when the starting composition is rich in Fe^{3+} (Table 1). At low temperatures of 400 and 500 °C, alluaudite crystals reach a diameter of 10–20 μm (Fig. 1a), while at 700 °C, the crystals can attain 50–100 μm (Fig. 1b, c, d). These large crystals are idiomorphic and show a dark green to brownish pleochroism (Fig. 1c, d). Average electron-microprobe compositions (Tables 2, 3) were plotted in several diagrams, in order to establish the substitution mechanisms affecting Fe-rich alluaudites. As shown in Figure 2, it is impossible to determine a unique substitution mechanism; however, two separate trends have been identified on the diagrams. The first trend is shown as solid lines in Figure 2; it corresponds to the substitution mechanism $3\ Fe^{2+} = 2\ Fe^{3+} + \square$. The second trend is shown as a dotted line; it corresponds to the substitution mechanism $2\ Fe^{2+} = Fe^{3+} + Na^+$, responsible for the variation in the Na contents in these phosphates. The chemical composition of the alluaudite-type phosphate, located at the intersection between these trends, corresponds to $\square_{0.5}Na_{1.5}Fe^{2+}{}_3Fe^{3+}{}_{0.5}(PO_4)_3$ (Fig. 2); this composition is the most Fe^{2+}-rich alluaudite synthesized in this study. Starting from this composition, the first trend evolves towards Fe^{3+}-rich $\square_{0.667}Na_{1.5}Fe^{2+}Fe^{3+}{}_{1.833}(PO_4)_3$, and the second trend evolves towards the Na- and Fe^{3+}-rich $Na_3Fe^{3+}{}_2(PO_4)_3$ composition (Fig. 2).

Sarcopside-type phosphates

Sarcopside, ideally $Fe^{2+}{}_3(PO_4)_2$, shows a crystal structure similar to that of olivine and of phosphates of the triphylite group [*a* 6.026 (8), *b* 4.768(9), *c* 10.44(2) Å, β 90.0(2)°, $P2_1/c$; Moore 1972]. The structure can be compared to an olivine structure in which Si^{4+} is replaced by P^{5+}. Consequences of this substitution are the presence of vacancies at one-third of the M1 positions, as well as strong octahedral distortions induced by bond-valence requirements. These octahedral distortions provoke a marked ordering of Fe at the M1 site, and of Mn at the M2 site, in members of the sarcopside-zavalíaite solid solution (Hatert *et al.* 2012).

Sarcopside-type phosphates have been observed in many hydrothermal experiments performed in this study, starting from Fe^{2+}-rich compositions (Table 1). In sample H.247, sarcopside grains are smaller than 50 μm, show an irregular shape, and form an intimate intergrowth with alluaudite and $Fe^{2+}{}_3(PO_4)_2 \bullet nH_2O$

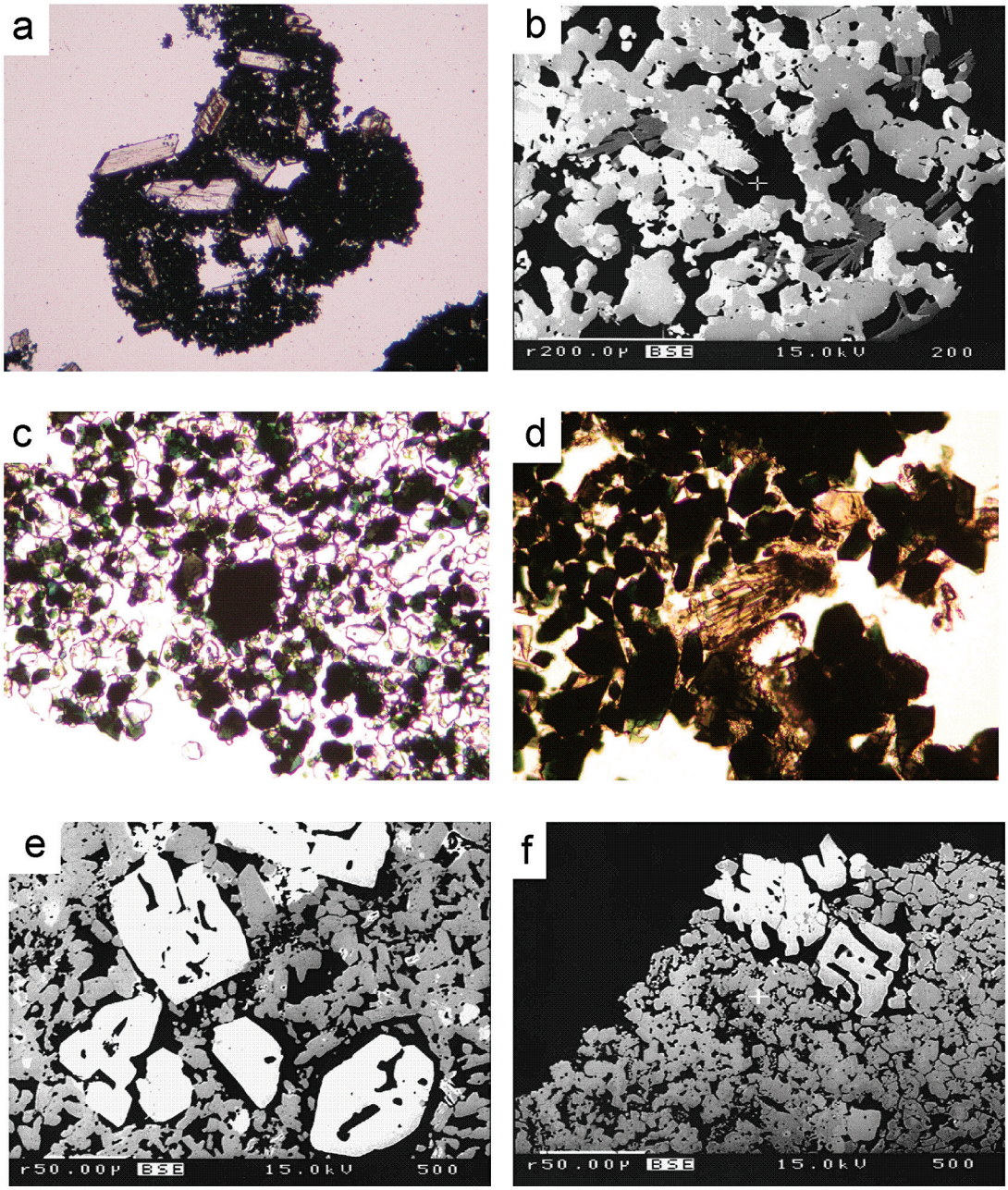

FIG. 1. (a) Large, idiomorphic, colorless crystals of $Fe_2P_2O_7$, associated with minute alluaudite grains forming black aggregates (sample H.253, plane polarized light; the long edge of the photograph is approximately 1 mm). (b) Intergrowth of alluaudite (medium gray) and sarcopside (light gray) grains, associated with elongated crystals of $Fe_3(PO_4)_2.nH_2O$ (dark gray) (sample H.278, scanning electron microscope, backscattered electron image). (c) Dark green crystals of alluaudite, associated with colorless grains of marićite (sample H.277, plane polarized light. The long edge of the photograph is approximately 500 µm). (d) Large, green, idiomorphic crystals of alluaudite, associated with brownish elongated crystals of X-phase (sample H.283, plane polarized light; the long edge of the photograph is approximately 500 µm). (e) Large idiomorphic sarcopside crystals (light gray), surrounded by $Fe^{2+}{}_3Fe^{3+}{}_4(PO_4)_6$ grains (dark gray) (sample H.228, scanning electron microscope, back-scattered electron image). (f) Large myrmekitic sarcopside crystal (light gray), surrounded by $Fe^{2+}{}_3Fe^{3+}{}_4(PO_4)_6$ grains (dark gray) (sample H.247, scanning electron microscope, back-scattered electron image).

needles (Fig. 1b). Sample H.228 shows large idiomorphic sarcopside grains associated with $Fe^{2+}{}_3Fe^{3+}{}_4(PO_4)_6$ (Fig. 1e); such large grains frequently show a characteristic myrmekitic texture (Figs. 1e, 1f, 3a). Electron-microprobe analyses (Table 3) are in very good agreement with the ideal composition of sarcopside, with Fe^{2+} between 2.97 and 3.11 atoms per formula unit (*apfu*).

Maricite-type phosphates

The crystal structure of maricite, $NaFe^{2+}(PO_4)$, was described by Le Page & Donnay (1977) [*a* 6.861(1), *b* 8.987(1), *c* 5.045(1) Å, *Pmnb*]; it is significantly different from that of karenwebberite, which is a polymorph of maricite showing the triphylite structure (Vignola *et al*. 2013). The maricite structure, which is more compact than the olivine structure, contains chains of edge-sharing *M*1 octahedra, oriented parallel to the *a* axis and occupied by Fe^{2+}. Each *M*1 octahedron shares some faces with the *M*2 polyhedra, which contain 10-coordinated Na. In the maricite structure, the *M*1 chains are identical to those of triphylite, but the *M*2 octahedral site is much larger than the *M*2 site of karenwebberite.

Maricite-type phosphates were formed in some of the hydrothermal experiments conducted in the present study and are frequently associated with alluaudite in the Fe^{2+}-rich experiments (Table 1). Maricite forms colorless grains reaching 50 μm, with an irregular and frequently rounded shape (Figs. 1c, 3c). The electron-microprobe analyses (Table 3) show compositions in very good agreement with the ideal stoichiometry of maricite.

$Fe^{3+}{}_4(PO_4)_3(OH)_3$

This compound was synthesized by Schmid-Beurmann (2000, 2001) during an investigation of the quaternary $FeO–Fe_2O_3–P_2O_5–H_2O$ system at 386 and 586 °C (*P* = 3 kbar). Its structure (Torardi *et al*. 1989) was solved in space group *C*2/*c* [*a* 19.555 (2), *b* 7.376(1), *c* 7.429(1) Å, β 102.26(1)°], and can be described as double chains of face-sharing FeO_6 octahedra, forming layers. In each layer, the chains are oriented perpendicular to those of adjacent layers; layers are interconnected by sharing corners of FeO_6 octahedra or *via* PO_4 tetrahedra. One-third of the Fe octahedra are vacant, thus dividing the chains into dimers of octahedra, separated by the vacant positions.

In the experiments located on the Fe^{3+}-rich side of the Na–Fe^{2+}–Fe^{3+} (+PO_4) system, $Fe^{3+}{}_4(PO_4)_3(OH)_3$ forms black crystals, associated with $Fe^{3+}{}_4(P_2O_7)_3$ and/or with $Fe^{2+}{}_3Fe^{3+}{}_4(PO_4)_6$. The crystals are fine-grained at 400 and 500 °C, but can reach 100 μm at 700 °C. Electron-microprobe compositions (Table 4), calculated on the basis of 3 P atoms *pfu* show significant variations of the OH (2.86–4.20 OH *pfu*) and Fe^{3+} (3.95–4.40 *apfu*) contents. Sodium also occurs in this phase, in amounts reaching 0.58 wt.% Na_2O.

$Fe^{2+}{}_3Fe^{3+}{}_4(PO_4)_6$

$Fe^{2+}{}_3Fe^{3+}{}_4(PO_4)_6$ was reported by Schmid-Beurmann (2001) as an intermediate phase between sarcopside and $Fe^{3+}{}_4(PO_4)_3(OH)_3$, in the quaternary $FeO–Fe_2O_3–P_2O_5–H_2O$ system, at 386 and 586 °C and 3 kbar. The crystal structure of this phosphate has been solved in space group $P\bar{1}$ [*a* 6.361(1), *b* 7.975(1), *c* 9.322(2) Å, α 105.27(1), β 108.06(1), γ 101.99(1)°], and is characterized by isolated PO_4 tetrahedra and four different types of Fe polyhedra. Fe1, Fe2, and Fe3 occur in octahedral environments, whereas Fe4 occurs in a fivefold distorted trigonal bipyramid. Fe1, Fe2, and Fe4 are connected to each other by edge sharing to form infinite chains parallel to the [101] direction; the chains

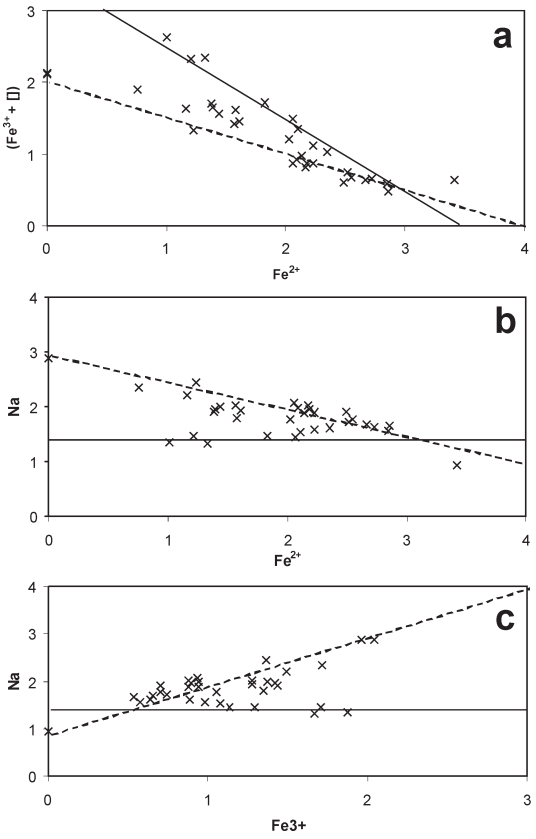

FIG. 2. Correlations between the major elements in Fe-rich alluaudite-type phosphates, synthesized in the Na–Fe^{2+}–Fe^{3+} (+ PO_4) system. The solid line corresponds to the substitution mechanism 3 Fe^{2+} = 2 Fe^{3+} + □, and the dotted line corresponds to the substitution mechanism 2 Fe^{2+} = Fe^{3+} + Na^+.

TABLE 2. CHEMICAL ANALYSES OF ALLUAUDITE-TYPE PHOSPHATE MINERALS, HYDROTHERMALLY SYNTHESIZED IN THE Na–Fe^{2+}–Fe^{3+} (+PO_4) SYSTEM

Experiment no. Number of analyses	H.219 (10)	H.222 (13)	H.223 (10)	H.224 (12)	H.227 (9)	H.241 (9)	H.242 (6)	H.253 (6)	H.254 (6)	H.255 (5)	H.256 (6)	H.257 (7)
P_2O_5	44.33	45.94	43.66	44.87	44.11	42.54	42.59	41.44	42.70	42.68	42.16	42.40
Fe_2O_3[a]	23.95	35.13	22.05	28.70	27.67	20.45	20.47	10.98	17.31	20.70	18.02	13.95
FeO[a]	20.67	-	23.26	18.34	19.74	23.09	22.51	35.65	30.32	26.33	29.37	31.90
Na_2O	12.32	19.24	11.44	9.52	8.51	11.99	12.52	10.73	9.61	9.06	8.90	11.70
Total (wt. %)	101.27	100.31	100.41	101.43	100.03	98.07	98.09	98.80	99.94	98.77	98.45	99.95
Cation numbers *pfu*												
P	3.000	3.000	3.000	3.000	3.000	3.000	3.000	3.000	3.000	3.000	3.000	3.000
Fe^{3+}	1.441	2.039	1.347	1.706	1.672	1.282	1.281	0.706	1.081	1.293	1.139	0.878
Fe^{2+}	1.382	-	1.579	1.211	1.326	1.609	1.566	2.549	2.104	1.828	2.064	2.230
Na	1.909	2.877	1.800	1.457	1.326	1.937	2.020	1.779	1.546	1.459	1.450	1.896
□	0.268	0.084	0.274	0.626	0.676	0.172	0.133	–0.034	0.269	0.420	0.347	–0.004
Experiment no. Number of analyses	H.258 (6)	H.259 (7)	H.260 (8)	H.264 (6)	H.265 (6)	H.268 (6)	H.269 (6)	H.270 (7)	H.273 (6)	H.274 (6)	H.277 (6)	H.278 (7)
P_2O_5	42.30	44.11	43.92	42.58	42.84	41.62	41.79	41.85	42.45	42.72	42.64	41.57
Fe_2O_3[a]	13.92	22.71	23.40	16.87	21.93	8.41	10.33	10.05	15.03	15.13	14.27	9.05
FeO[a]	30.93	21.43	20.62	29.09	17.78	40.13	37.60	38.47	30.62	30.08	31.33	39.88
Na_2O	12.48	12.83	12.49	10.98	15.20	10.06	10.26	9.88	11.61	12.34	12.14	9.50
Total (wt. %)	99.63	101.08	100.43	99.52	97.75	100.22	99.98	100.25	99.71	100.27	100.38	100.00
Cation numbers *pfu*												
P	3.000	3.000	3.000	3.000	3.000	3.000	3.000	3.000	3.000	3.000	3.000	3.000
Fe^{3+}	0.877	1.373	1.421	1.056	1.365	0.539	0.659	0.641	0.945	0.945	0.893	0.580
Fe^{2+}	2.167	1.440	1.391	2.024	1.230	2.858	2.666	2.724	2.138	2.087	2.178	2.843
Na	2.026	1.999	1.954	1.772	2.438	1.661	1.687	1.622	1.879	1.985	1.956	1.570
□	–0.070	0.188	0.234	0.148	–0.033	–0.058	–0.012	0.013	0.038	–0.017	–0.027	0.007

Analysts H.-J. Bernhardt (Bochum, Germany) and P. de Parseval (Toulouse, France). Cation numbers were calculated on the basis of 3 P per formula unit.
[a] The FeO and Fe_2O_3 values have been calculated to maintain charge balance.

are connected together by sharing octahedral corners with the $Fe3O_6$ octahedra and with the PO_4 tetrahedra (Lightfoot & Cheetham 1989, Dal Bo & Hatert 2012).

This phosphate was identified in several experiments located in the Fe-rich portions of the ternary system investigated herein, mainly those starting from compositions $Fe^{3+}(PO_4)$ and $Fe^{2+}{}_3(PO_4)_2$ (Table 1). This phase forms black crystals associated with large sarcopside grains (Fig. 1e,f), or it occurs as rounded black inclusions in a matrix of fine-grained $Fe^{3+}{}_4(P_2O_7)_3$ (Fig. 3b). Electron-microprobe compositions (Table 4) show a variable $Fe^{3+}/(Fe^{2+} + Fe^{3+})$ ratio, from 0.580 to 0.373, as well as a significant Na content, which reaches 1.67 wt.% Na_2O in sample H.256. The presence of Na in these phosphates was previously reported by Redhammer *et al.* (2004), who measured 0.32 wt.% Na_2O in their synthetic crystals.

$Fe^{2+}{}_2(P_2O_7)$ and $Fe^{3+}{}_4(P_2O_7)_3$

The $Fe^{2+}{}_2(P_2O_7)$ compound has a crystal structure similar to that of thortveitite, $Sc_2Si_2O_7$; it was solved by Stefanidis & Nord (1982) in space group *P*1 [*a* 5.517(2), *b* 5.255(2), *c* 4.488(1) Å, α 98.73(2), β 98.33(4), γ 103.81(2)°]. The structure is based on two types of FeO_6 octahedra, which share edges to form six-membered rings; the center of each ring is occupied by the P_2O_7 group. In the rings, each octahedron shares three of its edges with three adjacent octahedra. $Fe^{3+}{}_4(P_2O_7)_3$ is monoclinic, space group $P2_1/n$ [*a* 7.389(2), *b* 21.337(1), *c* 9.517(2) Å, β 90(1)°]; its crystal structure was described by Elbouaanani *et al.* (2002). The main feature of this structure is the occurrence of Fe_2O_9 dimers made up of face-sharing FeO_6 octahedra. The dimers are connected by sharing corners with the tetrahedral sites to form infinite (010) layers

containing the Fe sites; these layers are interconnected in the *b* direction *via* the P_2O_7 groups.

$Fe^{2+}{}_2(P_2O_7)$ forms colorless idiomorphic crystals reaching 200 μm in length, associated with minute black alluaudite crystals (Fig. 1a), whereas $Fe^{3+}{}_4(P_2O_7)_3$ forms tiny colorless grains associated with $Fe^{2+}{}_3Fe^{3+}{}_4(PO_4)_6$ (Fig. 3b) and $Fe^{3+}{}_4(PO_4)_3(OH)_3$ in Fe^{3+}-rich experiments (Table 1). Electron-microprobe compositions of these diphosphates (Table 4) are in very good agreement with their ideal compositions, except for some minor amounts of Na, reaching 0.20 wt.% Na_2O in $Fe^{2+}{}_2(P_2O_7)$.

$Fe_3(PO_4)_2{\cdot}nH_2O$

A brownish phosphate, forming elongated crystals reaching 150 μm in length, was observed in experiment H.278 performed at 700 °C; it is associated with alluaudite and sarcopside grains (Fig. 1b). This phase appears dark gray in backscattered electron microscopy, indicating that it contains a significant amount of water. This hypothesis is confirmed by the low total of the electron-microprobe analysis (Table 4). The presence of water in similar crystals, obtained experimentally by Hatert *et al.* (2011), was confirmed by SIMS analyses.

TABLE 3. CHEMICAL ANALYSES OF ALLUAUDITE-, MARIĆITE-, AND SARCOPSIDE-TYPE PHOSPHATES, HYDROTHERMALLY SYNTHESIZED IN THE Na–Fe^{2+}–Fe^{3+} (+PO_4) SYSTEM

	alluaudite										sarcopside					
Experiment no.	H.279	H.280	H.283	H.284	H.287	H.315	H.317	H.317	H.318	H.318	H.228	H.247	H.248	H.268	H.270	H.278
Number of analyses	(6)	(6)	(7)	(8)	(6)	(9)	(9)	(7)	(9)	(6)	(11)	(10)	(5)	(4)	(5)	(6)
P_2O_5	42.38	42.33	41.96	42.11	42.61	43.96	45.90	46.29	45.12	43.64	40.29	38.82	38.80	39.39	38.81	38.44
Fe_2O_3[a]	15.67	14.14	11.10	11.74	14.99	30.88	29.48	34.15	25.24	20.10	-	-	-	-	-	-
FeO[a]	31.88	33.58	35.27	35.79	29.60	14.98	11.72	-	17.71	32.22	60.59	60.39	60.57	60.45	60.70	60.54
Na_2O	9.73	9.97	11.60	10.59	12.81	8.70	15.69	19.42	14.45	5.98	-	-	-	-	-	-
H_2O[a]	-	-	-	-	-	-	-	0.42	-	-	-	-	-	-	-	-
Total (wt.%)	99.66	100.02	99.93	100.23	100.01	98.52	102.79	100.28	102.52	101.94	100.88	99.21	99.37	99.84	99.51	98.98
Cation numbers *pfu*																
P	3.000	3.000	3.000	3.000	3.000	3.000	3.000	3.000	3.000	3.000	2.000	2.000	2.000	2.000	2.000	2.000
Fe^{3+}	0.986	0.891	0.705	0.743	0.938	1.873	1.713	1.967	1.492	1.228	-	-	-	-	-	-
Fe^{2+}	2.229	2.351	2.491	2.519	2.058	1.010	0.757	-	1.163	2.187	2.971	3.073	3.085	3.032	3.090	3.111
Na	1.578	1.619	1.900	1.729	2.065	1.360	2.349	2.883	2.199	0.942	-	-	-	-	-	-
H	-	-	-	-	-	-	-	0.215	-	-	-	-	-	-	-	-
□	0.139	0.139	–0.096	0.009	–0.061	0.757	0.181	0.150	0.146	0.643	-	-	-	-	-	-

	Sarc.	maricite														
Experiment no.	H.281	H.217	H.218	H.219	H.258	H.261	H.262	H.263	H.264	H.268	H.273	H.274	H.277	H.283	H.285	H.287
Number of analyses	(6)	(8)	(6)	(6)	(4)	(7)	(5)	(4)	(4)	(6)	(5)	(4)	(5)	(5)	(4)	(4)
P_2O_5	39.07	41.77	41.74	41.86	40.70	39.67	40.15	39.54	40.16	40.44	40.69	40.75	40.48	41.14	40.84	40.64
FeO	60.51	41.89	41.67	41.81	41.33	41.76	41.67	42.12	41.78	42.51	41.92	41.93	41.78	41.86	41.82	41.90
Na_2O	-	17.64	17.57	17.70	17.77	17.86	17.76	17.73	17.71	17.52	17.88	17.74	17.76	17.92	17.81	17.82
Total (wt.%)	99.58	101.30	100.98	101.37	99.8	99.29	99.58	99.39	99.65	100.47	100.49	100.42	100.02	100.92	100.47	100.36
Cation numbers *pfu*																
P	2.000	1.000	1.000	1.000	1.000	1.000	1.000	1.000	1.000	1.000	1.000	1.000	1.000	1.000	1.000	1.000
Fe^{2+}	3.059	0.991	0.986	0.987	1.004	1.040	1.025	1.052	1.028	1.038	1.018	1.016	1.020	1.005	1.012	1.018
Na	-	0.967	0.964	0.968	0.987	1.031	1.013	1.027	1.010	0.992	1.006	0.997	1.005	0.998	0.999	1.004

Analysts H.-J. Bernhardt (Bochum, Germany) and P. de Parseval (Toulouse, France). Cation numbers calculated on the basis of 1 P (maricite), 2 P (sarcopside), and 3 P atoms (alluaudite) per formula unit. [a] The FeO, Fe_2O_3, and H_2O values have been calculated to maintain charge balance.

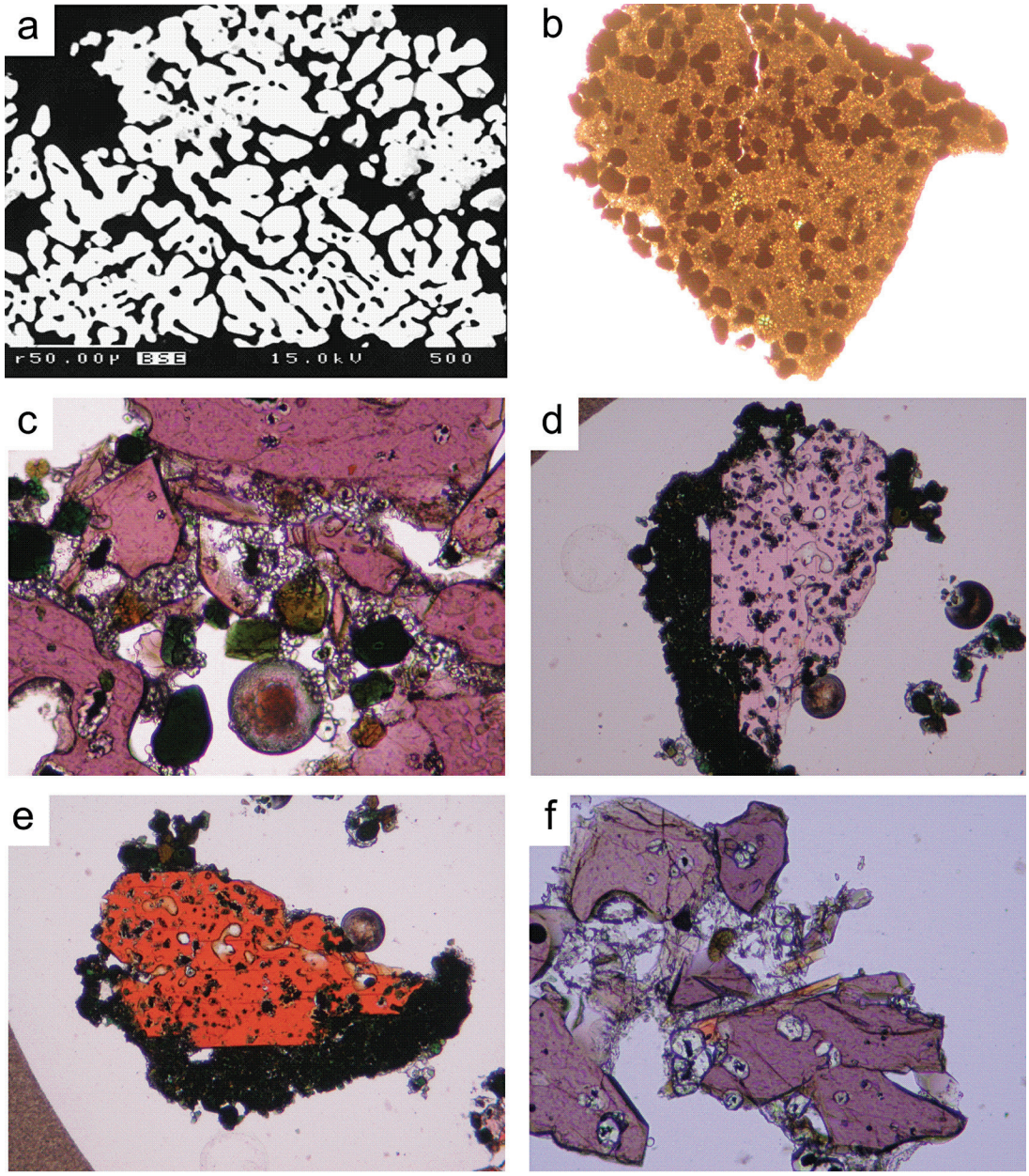

FIG. 3. (a) Large myrmekitic sarcopside grain (sample H.281, scanning electron microscope, back-scattered electron image). (b) Large black crystals of $Fe^{2+}{}_3Fe^{3+}{}_4(PO_4)_6$, surrounded by a matrix of fine-grained $Fe^{3+}{}_4(P_2O_7)_3$ (sample H.282, plane polarized light; the long edge of the photograph is approximately 1 mm). (c) Large pink crystals of $Na_4Fe^{2+}Fe^{3+}(PO_4)_3$, associated with tiny grains of colorless maricite and with $Na_7Fe^{2+}Fe^{3+}{}_3(PO_4)_6$ green, idiomorphic crystals. The strong pleochroism of $Na_7Fe^{2+}Fe^{3+}{}_3(PO_4)_6$, with colors from bottle green to pinkish brown, is clearly visible (sample H.261, plane polarized light; the long edge of the photograph is approximately 500 μm). (d) Large crystal of $Na_2Fe^{3+}(PO_4)(HPO_4)\bullet H_2O$, showing a light pink color and a perfect cleavage plane parallel to the elongation. The black aggregates surrounding this crystal are composed of$Na_7Fe^{2+}Fe^{3+}{}_3(PO_4)_6$ (sample H.263, plane polarized light; the long edge of the photograph is approximately 1 mm). (e) The crystal of Figure 1d, observed after a rotation of 90°. The strong pleochroism, from light pink to deep orange, is clearly visible. (f) Large pink crystals of $Na_4Fe^{2+}Fe^{3+}(PO_4)_3$, associated with tiny grains of colorless maricite and with an orange elongated crystal of $Na_3Fe^{3+}(PO_4)_2$ (sample H.262, plane polarized light; the long edge of the photograph is approximately 500 μm).

TABLE 4. CHEMICAL ANALYSES OF IRON PHOSPHATES, HYDROTHERMALLY SYNTHESIZED IN THE Na-Fe^{2+}-Fe^{3+} (+PO_4) SYSTEM

	$Fe^{3+}_4(PO_4)_3(OH)_3$						$Fe^{2+}_2(P_2O_7)$					
Experiment no.	H.224	H.227	H.255	H.271	H.272	H.282	H.253	H.254	H.279	H.280	H.284	H.282
Number of analyses	(3)	(9)	(10)	(6)	(6)	(5)	(6)	(6)	(4)	(6)	(4)	(5)
P_2O_5	37.83	37.60	35.96	38.44	37.82	37.66	47.38	49.21	49.13	49.31	49.21	49.16
Fe_2O_3[a]	59.02	56.48	59.27	56.96	57.83	57.89	-	-	-	-	-	-
FeO[a]	-	-	-	-	-	-	51.07	50.60	50.61	50.57	50.73	50.86
Na_2O	0.58	0.32	0.09	0.00	-	-	-	0.10	0.02	0.02	0.20	-
H_2O[a]	5.73	4.89	6.39	4.64	5.17	5.25	-	-	-	-	-	-
Total (wt.%)	103.16	99.29	101.71	100.04	100.82	100.80	98.45	99.91	99.76	99.90	100.14	100.02
Cation numbers *pfu*												
P	3.000	3.000	3.000	3.000	3.000	3.000	2.000	2.000	2.000	2.000	2.000	2.000
Fe^{3+}	4.161	4.005	4.395	3.952	4.078	4.100	-	-	-	-	-	-
Fe^{2+}	-	-	-	-	-	-	2.130	2.031	2.035	2.026	2.037	2.044
Na	0.105	0.059	0.018	-	-	-	-	0.009	0.001	0.002	0.019	-
H^+	3.587	3.075	4.202	2.855	3.233	3.299	-	-	-	-	-	-

	$Fe^{2+}_3Fe^{3+}_4(PO_4)_6$								$Fe^{3+}_4(P_2O_7)_3$		$Fe^{2+}_3(PO_4)_2 \cdot nH_2O$
Experiment no.	H.227	H.228	H.247	H.248	H.256	H.271	H.272	H.282	H.272	H.282	H.278
Number of analyses	(17)	(10)	(6)	(6)	(6)	(6)	(6)	(7)	(6)	(5)	(8)
P_2O_5	44.42	44.86	43.39	43.15	42.09	43.94	43.81	43.91	55.03	53.95	29.52
Fe_2O_3[a]	30.82	34.03	29.02	27.27	21.63	31.69	29.90	30.33	42.51	41.63	-
FeO[a]	24.05	22.16	26.67	28.62	32.76	23.45	26.03	25.69	-	-	45.29
Na_2O	1.52	0.01	0.02	0.05	1.67	0.03	0.06	0.01	-	-	0.18
H_2O[a]	-	-	-	-	-	-	-	-	-	-	25.01
Total (wt.%)	100.81	101.06	99.10	99.09	98.15	99.11	99.80	99.94	97.54	95.58	100.00
Cation numbers *pfu*											
P	6.000	6.000	6.000	6.000	6.000	6.000	6.000	6.000	6.000	6.000	2.000
Fe^{3+}	3.701	4.046	3.567	3.371	2.740	3.846	3.640	3.683	4.120	4.115	-
Fe^{2+}	3.209	2.928	3.643	3.931	4.613	3.163	3.521	3.467	-	-	3.031
Na	0.470	0.002	0.008	0.016	0.544	0.010	0.018	0.004	-	-	0.029
H	-	-	-	-	-	-	-	-	-	-	13.36

Analysts H.-J. Bernhardt (Bochum, Germany) and P. de Parseval (Toulouse, France). Cation numbers calculated on the basis of 2 P ($Fe^{2+}_2(P_2O_7)$, $Fe^{2+}_3(PO_4)_2 \cdot nH_2O$), 3 P ($Fe^{3+}_4(PO_4)_3(OH)_3$), and 6 P atoms ($Fe^{2+}_3Fe^{3+}_4(PO_4)_6$, $Fe^{3+}_4(P_2O_7)_3$) per formula unit.
[a] The FeO, Fe_2O_3, and H_2O values have been calculated to maintain charge balance.

Several X-ray diffraction peaks, observed in the powder pattern of sample H.278, indicate that this phosphate certainly shows a crystal structure similar to that of laueite, $(Fe^{3+},Mn)_3(PO_4)_2(OH)_2.8H_2O$

$Na_7Fe^{2+}Fe^{3+}{}_3(PO_4)_6$

The crystal structure of this phosphate was solved in space group $R\bar{3}c$ [*a* 13.392(2), *c* 17.858(3) Å] by Lii (1996); it contains four FeO_6 octahedra and six PO_4 tetrahedra. The building unit of the structure consists of an octahedral tetramer with a central Fe(1)O_6 octahedron sharing three of its edges with three Fe(2)O_6 octahedra. Each unit is connected to three units above and three units below to form a three-dimensional framework with large cavities containing Na atoms. $Na_7Fe^{2+}Fe^{3+}{}_3(PO_4)_6$ was observed in experiments performed at 400 and 500 °C from the starting composition $Na_4Fe^{2+}Fe^{3+}(PO_4)_3$ (Table 1); it forms idiomorphic green crystals associated with marićite, $Na_4Fe^{2+}Fe^{3+}(PO_4)_3$ (Fig. 3c), and $Na_2Fe^{3+}(PO_4)(HPO_4) \cdot H_2O$ (Fig. 3d). Electron-microprobe analyses (Table 5) indicate a chemical composition $Na_{7.06–7.17}Fe^{2+}{}_{1.57–1.66}Fe^{3+}{}_{2.50–2.60}(PO_4)_6$, in good agreement with the ideal formula of this phosphate.

$Na_4Fe^{2+}Fe^{3+}(PO_4)_3$

In two experiments performed at 500 (H.261) and 600 °C (H.262), starting from the composition $Na_4Fe^{2+}Fe^{3+}(PO_4)_3$, large pink crystals reaching 500 μm in diameter were synthesized. The crystals show an irregular shape, and their pink color is clearly visible under the polarizing microscope (Fig. 3c, f). The main

TABLE 5. CHEMICAL ANALYSES OF SODIUM AND SODIUM-IRON PHOSPHATES, HYDROTHERMALLY SYNTHESIZED IN THE Na–Fe^{2+}–Fe^{3+} (+PO_4) SYSTEM

	$Na_7Fe^{2+}Fe^{3+}{}_3(PO_4)_6$		$Na_4Fe^{2+}Fe^{3+}(PO_4)_3$		$Na_3Fe^{3+}(PO_4)_2$		$Na_{4-2x}Fe^{3+}(PO_4)_{2-x}(HPO_4)_x(OH)_{1-x}\bullet xH_2O$	
Run no.	H.261	H.263	H.261	H.262	H.262	H.285	H.262	H.263
Number of analyses	(6)	(7)	(6)	(6)	(6)	(8)	(3)	(7)
P_2O_5	43.76	43.88	42.47	42.91	44.36	44.92	44.40	44.08
Fe_2O_3[a]	20.54	21.36	14.17	13.81	24.94	26.16	26.29	26.46
FeO[a]	12.24	11.65	16.94	17.31	-	-	-	-
Na_2O	22.82	22.56	24.47	25.19	27.39	28.33	18.08	19.61
H_2O[a]	-	-	-	-	0.48	0.02	8.38	7.72
Total (wt. %)	99.36	99.45	98.05	99.22	97.17	99.43	97.15	97.87
Cation numbers *pfu*								
P	6.000	6.000	3.000	3.000	2.000	2.000	2.000	2.000
Fe^{3+}	2.504	2.595	0.889	0.858	1.000	1.035	1.052	1.067
Fe^{2+}	1.658	1.573	1.182	1.196	-	-	-	-
Na	7.165	7.063	3.958	4.033	2.829	2.889	1.866	2.037
H	-	-	-	-	0.171	0.005	2.977	2.761

	X-phase	$NaFe^{3+}(P_2O_7)$				$Na_2HPO_4\bullet nH_2O$			
Run no.	H.283	H.241	H.242	H.256	H.259	H.262	H.263	H.264	H.285
Number of analyses	(6)	(5)	(6)	(7)	(6)	(3)	(6)	(8)	(3)
P_2O_5	41.44	54.13	52.49	52.64	54.44	47.16	45.22	42.88	44.34
Fe_2O_3[a]	10.64	32.47	33.01	32.54	31.93	-	-	-	-
FeO[a]	37.26	-	-	-	-	0.25	0.79	6.15	0.38
Na_2O	9.74	12.31	12.33	12.41	12.79	44.03	41.29	36.82	36.92
H_2O[a]	-	-	-	-	-	8.56	12.70	14.15	18.36
Total (wt. %)	99.08	98.91	97.83	97.59	99.16	100.00	100.00	100.00	100.00
Cation numbers *pfu*									
P	6.000	2.000	2.000	2.000	2.000	1.000	1.000	1.000	1.000
Fe^{3+}	1.369	1.066	1.118	1.099	1.043	-	-	-	-
Fe^{2+}	5.329	-	-	-	-	0.005	0.017	0.142	0.008
Na	3.230	1.042	1.076	1.080	1.076	2.138	2.091	1.966	1.907
H	-	-	-	-	-	1.431	2.215	2.602	3.265

Analysts H.-J. Bernhardt (Bochum, Germany) and P. de Parseval (Toulouse, France). Cation numbers were calculated on the basis of 1 P ($Na_2HPO_4\bullet nH_2O$), 2 P [$Na_3Fe^{3+}(PO_4)_2$, $Na_{4-2x}Fe^{3+}(PO_4)_{2-x}(HPO_4)_x(OH)_{1-x}\bullet xH_2O$, $NaFe^{3+}(P_2O_7)$], 3 P [$Na_4Fe^{2+}Fe^{3+}(PO_4)_3$], and 6 P atoms [$Na_7Fe^{2+}Fe^{3+}{}_3(PO_4)_6$, X-phase] per formula unit.
[a] The FeO, Fe_2O_3, and H_2O values have been calculated to maintain charge balance.

associated phosphates are marićite, $Na_7Fe^{2+}Fe^{3+}{}_3(PO_4)_6$ (Fig. 3c), and $Na_2Fe^{3+}(PO_4)(HPO_4)\bullet H_2O$ (Fig. 3f). Single-crystal X-ray diffraction measurements, performed by Hatert (2009) using these crystals, indicate that their structure is topologically related to that of NASICON-type ionic conductors [$R\bar{3}c$; a 8.9543(9), c 21.280(4) Å]. The heteropolyhedral framework is based on the regular alternation, in three dimensions, of corner-sharing PO_4 tetrahedra and FeO_6 octahedra. These polyhedra form so called 'lantern units', which are stacked along the c axis; the six- and eight-coordinated Na sites occur between two lantern units. The structural formula of this phase is $Na_4Fe^{2+}Fe^{3+}(PO_4)_3$; this formula is in good agreement with the electron-microprobe analyses (Table 5), which indicate an empirical composition $Na_{3.96–4.03}Fe^{2+}{}_{1.18–1.20}Fe^{3+}{}_{0.86–0.90}(PO_4)_3$.

$Na_3Fe^{3+}(PO_4)_2$

The two experiments performed at 600 (H.262) and 700 °C (H.285), starting from the composition $Na_4Fe^{2+}Fe^{3+}(PO_4)_3$, showed the presence of a brownish phosphate forming needles reaching 200 μm in length (Fig. 3f). These needles are associated with marićite,

$Na_4Fe^{2+}Fe^{3+}(PO_4)_3$ (Fig. 3f), and $Na_2Fe^{3+}(PO_4)(HPO_4)•H_2O$ (Table 1). Hatert (2007) performed single-crystal X-ray diffraction experiments on these needles, which are triclinic, space group $P\bar{1}$, *a* 5.3141(6), *b* 8.5853(9), *c* 8.7859(8) Å, α 114.429(9), β 92.327(9), γ 106.08(1)°. The fundamental structural unit of this compound is a double heteropolyhedral chain running along [100], a chain which is similar to that occurring in hannayite, $(NH_4)_2[Mg_3(PO_3OH)_4(H_2O)_8]$ (Catti & Franchini-Angela 1976). The parallel double chains, which are linked together by large Na cations, are formed by $Fe1O_6$ octahedra linked via corner-sharing to $P1O_4$ tetrahedra, and decorated by edge-sharing $P2O_4$ tetrahedra. The double chains can be described as two connected single chains, each of which shows a regular alternation of octahedra and tetrahedra in a 1:1 ratio. Electron-microprobe analyses (Table 5) indicate a composition $Na_{2.83–2.90}Fe^{3+}{}_{1.00–1.04}(PO_4)_2$, in good agreement with the ideal formula of this phosphate.

$Na_{4–2x}Fe^{3+}(PO_4)_{2–x}(HPO_4)_x(OH)_{1–x}•xH_2O$

In sample H.263 we observed large orange crystals up to 1 mm in diameter, and characterized by an X-ray powder diffraction pattern distinct from those of known phosphate structures. This phase is associated with $Na_7Fe^{2+}Fe^{3+}{}_3(PO_4)_6$ and marićite in sample H.263 and with $Na_4Fe^{2+}Fe^{3+}(PO_4)_3$ and marićite in sample H.262 (Table 1). Under the polarizing microscope, perfect cleavage planes are observed parallel to the elongation of the crystals, as well as a strong pleochroism from pale pink (Fig. 3d) to deep orange (Fig. 3e).

Single-crystal X-ray measurements were performed on a crystal of this phase measuring 0.11 × 0.13 × 0.27 mm; they indicated the unit-cell parameters *a* 15.5004(8), *b* 7.1465(5), *c* 29.239(2)Å, *V* = 3238.9(3) Å^3, space group *Pnma*. The crystal structure (Fig. 4) was refined by direct methods with SHELXTL (Sheldrick 2008); scattering curves for neutral atoms, together with anomalous dispersion corrections, were taken from the *International Tables for X-ray Crystallography* (Wilson 1992). In the final refinement cycle, the occupancies of Na at the Na2 and Na10 sites were refined, and the occupancies of O and H at the O10 and H1 sites were constrained to 0.20. The refinements were completed using anisotropic displacement parameters for all non-hydrogen atoms. The final conventional R_1 factor [$F_o > 2\sigma(F_o)$] was 0.0395; further details on the intensity data collection and structure refinement are given in Table 6.

The structure of the title compound can be compared to that of the superionic conductor $Na_9Fe_2(PO_4)_4(O,F)_2$, synthesized by Maximov *et al*. (1994); however, the unit-cell parameters and space group reported by these authors are significantly different from those of our phosphate. Atomic coordinates (Table 7) indicate the presence of three Fe sites, eight P sites, and 11 Na sites in this complex structure (Fig. 4a). Interatomic distances (Table 8) show that Fe atoms occur at regular octahedral sites, with average Fe–O bond distances from 2.001 to 2.012 Å. Sodium atoms occur in five-coordinated (Na2, Na9, Na10), octahedral (Na3, Na6, Na8), or seven-coordinated (Na1, Na4, Na5, Na7, Na11) sites; the average Na–O bond distances are between 2.325 and 2.596 Å. The structure (Fig. 4) consists of FeO_6 octahedra sharing corners to form chains aligned along the *b* axis (Fig. 4c); the chains are decorated by tetrahedral sites which share two of their corners with corners of the octahedral sites (Fig. 4a). These chains show a topology identical to that characterizing the chains of the compound $Na_9Fe_2(PO_4)_4(O,F)_2$ (Maximov *et al*. 1994) and of jahnsite-type phosphates (Kampf *et al*. 2008). Between the chains occur NaO_{5-7} polyhedra; some NaO_6 octahedra share edges to form chains aligned along the *b* axis (Fig. 4a). A view along *b* (Fig. 4c) clearly shows that the chains are not connected to each other, since the remaining corners of tetrahedral sites are shared with Na atoms occurring between the chains.

The chemical composition, calculated from the structural data, corresponds to $Na_{8.27}Fe^{3+}{}_2(PO_4)_4(OH)_2$; it can be simplified to the formula $Na_4Fe^{3+}(PO_4)_2(OH)$. The electron-microprobe compositions, however, indicate a significantly lower Na content for these compounds, leading to the empirical formula $Na_{2.04}Fe^{3+}{}_{1.07}(HPO_4)_{0.88}(PO_4)_{1.12}(OH)_{0.12}·0.88H_2O$ (Table 5). In this formula, the deficit in Na is compensated by a

TABLE 6. EXPERIMENTAL DETAILS FOR THE SINGLE-CRYSTAL X-RAY DIFFRACTION STUDY OF $Na_4Fe^{3+}(PO_4)_2(OH)$

	$Na_4Fe^{3+}(PO_4)_2(OH)$
Color	Orange
Dimensions of the crystal (mm)	0.11 × 0.13 × 0.27
a (Å)	15.5004(8)
b (Å)	7.1465(5)
c (Å)	29.239(2)
V (Å^3)	3238.9(3)
Space group	*Pnma*
Z	8
$2\theta_{min.}$, $2\theta_{max}$	5.86°, 52.65°
Range of indices	$–12 \le h \le 19$, $–5 \le k \le 8$, $–36 \le l \le 35$
Measured intensities	10232
Unique reflections	3570
Independent non-zero [$I > 2\sigma(I)$] reflections	2548
μ (mm^{-1})	2.520
Refined parameters	358
R_1 [$F_o > 2\sigma(F_o)$]	0.0395
R_1 (all)	0.0618
wR_2 (all)	0.1156
S (goodness of fit)	1.061
Max Δ/σ in the last l.s. cycle	0.001
Max peak and hole in the final Δ*F* map (*e*/Å^3)	+0.751 and –0.425

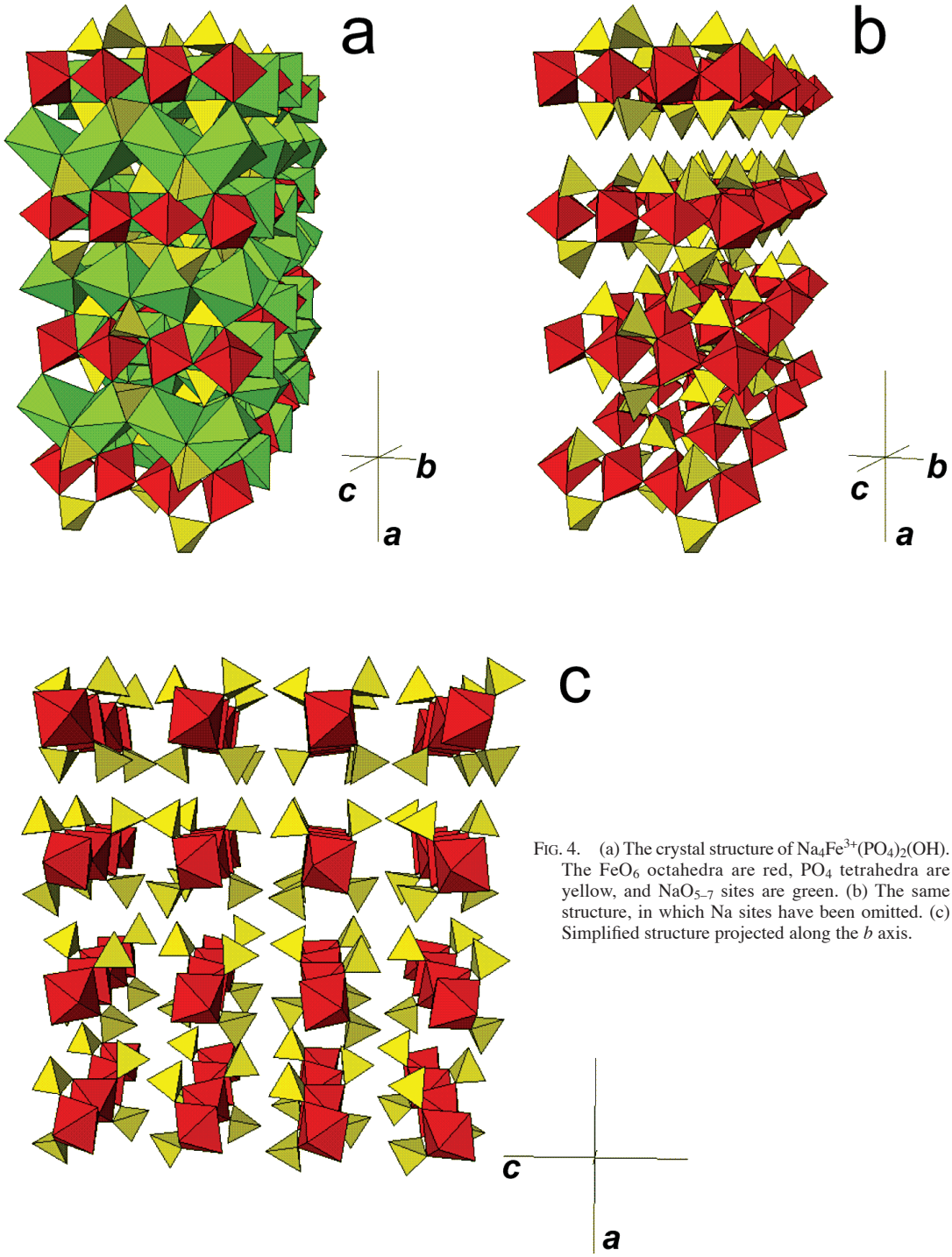

FIG. 4. (a) The crystal structure of $Na_4Fe^{3+}(PO_4)_2(OH)$. The FeO_6 octahedra are red, PO_4 tetrahedra are yellow, and NaO_{5-7} sites are green. (b) The same structure, in which Na sites have been omitted. (c) Simplified structure projected along the *b* axis.

TABLE 7. FINAL FRACTIONAL COORDINATES AND ISOTROPIC DISPLACEMENT PARAMETERS (Å^2) FOR $Na_4Fe^{3+}(PO_4)_2(OH)$

Site	*x*	*y*	*z*	$U_{eq.}$
Fe1	0.00252(3)	0.50658(7)	0.75010(2)	0.0130(2)
Fe2	0.50	0.50	0.50	0.0117(2)
Fe3	0	0	0.50	0.0125(2)
P1	0.86765(8)	0.25	0.68671(4)	0.0116(3)
P2	0.12815(8)	0.25	0.68407(4)	0.0123(3)
P3	0.37545(8)	0.75	0.43223(4)	0.0113(3)
P4	0.87573(8)	0.75	0.81750(5)	0.0134(3)
P5	0.36663(8)	0.25	0.55971(4)	0.0129(3)
P6	0.12352(8)	0.75	0.57006(5)	0.0134(3)
P7	0.86388(8)	0.75	0.56218(4)	0.0131(3)
P8	0.36093(8)	0.25	0.31302(4)	0.0118(3)
Na1	0.6277(1)	0.75	0.55845(7)	0.0211(5)
Na2*	0.3675(2)	0.25	0.1888(1)	0.020(1)
Na3	0.2448(1)	–0.0135(2)	0.38199(7)	0.0347(5)
Na4	0.9820(1)	0.0002(2)	0.62497(5)	0.0255(4)
Na5	0.3638(1)	0.75	0.30288(7)	0.0174(5)
Na6	0.7593(1)	0.0071(2)	0.76305(6)	0.0284(4)
Na7	0.4935(1)	0.5126(2)	0.37025(5)	0.0256(4)
Na8	0.2744(1)	0.9989(2)	0.62328(5)	0.0330(4)
Na9	0.1243(1)	0.25	0.56744(7)	0.0207(5)
Na10**	0.8673(2)	0.75	0.69340(9)	0.0193(9)
Na11	0.24668(9)	0.9797(2)	0.50687(6)	0.0236(4)
O1	0.5075(2)	0.75	0.2806(1)	0.0138(8)
O2	0.0058(2)	0.75	0.7222(1)	0.0197(9)
O3	–0.0060(2)	0.25	0.5307(1)	0.0159(8)
O4	0.0766(2)	0.25	0.6399(1)	0.0194(8)
O5	0.2254(2)	0.25	0.6754(1)	0.0189(8)
O6	0.7710(2)	0.75	0.5459(1)	0.029(1)
O7	–0.0896(2)	–0.0747(4)	0.5450(1)	0.0309(7)
O8	0.9015(2)	0.5720(4)	0.79067(9)	0.0210(6)
O9	0.3932(2)	0.9246(4)	0.21377(8)	0.0197(6)
O10***	0.869(1)	0.25	0.5566(7)	0.028(5)
O11	0.8669(2)	0.75	0.6144(1)	0.0259(9)
O12	0.8583(2)	0.25	0.6345(1)	0.0178(8)
O13	0.9178(2)	0.0715(4)	0.70051(8)	0.0176(6)
O14	0.2768(2)	0.25	0.2862(2)	0.030(1)
O15	0.3445(3)	0.25	0.3647(1)	0.0260(9)
O16	0.7789(2)	0.25	0.7100(1)	0.0232(9)
O17	0.0958(2)	0.9284(4)	0.54331(9)	0.0264(7)
O18	0.4173(3)	0.25	0.1170(1)	0.028(1)
O19	0.2220(2)	0.75	0.5713(1)	0.0220(9)
O20	0.4143(2)	0.4271(4)	0.30133(8)	0.0170(6)
O21	0.4263(2)	0.5719(4)	0.44565(8)	0.0171(6)
O22	0.7770(2)	0.75	0.8213(1)	0.0167(8)
O23	0.5843(2)	0.25	0.3651(1)	0.0229(9)
O24	0.4868(2)	0.75	0.5298(1)	0.0144(8)
O25	0.3671(2)	0.75	0.3802(1)	0.0176(8)
O26	0.2673(2)	0.25	0.5641(1)	0.0170(8)
O27	0.3916(2)	0.4241(4)	0.53143(9)	0.0190(6)
O28	0.2863(2)	0.75	0.4540(1)	0.0213(9)
O29	0.5929(2)	0.75	0.3932(1)	0.0214(9)
H1****	0.900(5)	0.1534(15)	0.551(7)	0.032

Occupancy factors : * 0.724(8) Na; ** 0.823(8) Na; *** 0.20 O; **** 0.20 H.

TABLE 8. SELECTED BOND DISTANCES (Å) FOR $Na_4Fe^{3+}(PO_4)_2(OH)$

P1–O12	1.534(4)	P2–O4	1.518(4)	P3–O21	1.548(3)	P4–O8	1.547(3)
P1–O13	1.547(3)	P2–O5	1.529(4)	P3–O21	1.548(3)	P4–O8	1.547(3)
P1–O13	1.547(3)	P2–O9	1.556(3)	P3–O25	1.528(3)	P4–O22	1.535(3)
P1–O16	1.534(4)	P2–O9	1.556(3)	P3–O28	1.521(4)	P4–O23	1.523(4)
Mean	1.541	Mean	1.540	Mean	1.536	Mean	1.538
P5–O26	1.544(3)	P6–O17	1.556(3)	P7–O6	1.517(4)	P8–O14	1.522(4)
P5–O27	1.543(3)	P6–O17	1.556(3)	P7–O7	1.530(3)	P8–O15	1.533(4)
P5–O27	1.543(3)	P6–O18	1.512(4)	P7–O7	1.530(3)	P8–O20	1.550(3)
P5–O29	1.513(4)	P6–O23	1.527(4)	P7–O11	1.526(4)	P8–O20	1.550(3)
Mean	1.536	Mean	1.538	Mean	1.526	Mean	1.539
Fe1–O1	2.044(2)	Fe2–O21	2.023(2)	Fe3–O3	2.001(2)	Na1–O6	2.251(4)
Fe1–O2	1.923(2)	Fe2–O21	2.023(2)	Fe3–O3	2.001(2)	Na1–O15	2.288(4)
Fe1–O8	2.019(2)	Fe2–O24	1.999(2)	Fe3–O7	1.986(3)	Na1–O21	2.451(3)
Fe1–O9	2.021(2)	Fe2–O24	1.999(2)	Fe3–O7	1.986(3)	Na1–O21	2.451(3)
Fe1–O13	2.034(2)	Fe2–O27	1.990(2)	Fe3–O17	2.017(2)	Na1–O24	2.338(4)
Fe1–O20	2.033(2)	Fe2–O27	1.990(2)	Fe3–O17	2.017(2)	Na1–O27	2.923(3)
Mean	2.012	Mean	2.004	Mean	2.001	Na1–O27	2.923(3)
						Mean	2.518
Na2–O2	2.193(5)	Na3–O6	2.837(3)	Na4–O4	2.351(3)	Na5–O1	2.321(4)
Na2–O9	2.469(3)	Na3–O11	2.560(3)	Na4–O7	2.644(3)	Na5–O9	2.925(3)
Na2–O9	2.469(3)	Na3–O12	2.376(3)	Na4–O11	2.546(3)	Na5–O9	2.925(3)
Na2–O18	2.237(5)	Na3–O15	2.488(3)	Na4–O12	2.635(3)	Na5–O16	2.243(4)
Na2–O22	2.258(4)	Na3–O25	2.540(3)	Na4–O13	2.476(3)	Na5–O20	2.437(3)
Mean	2.325	Na3–O28	2.776(3)	Na4–O17	3.01(3)	Na5–O20	2.437(3)
		Mean	2.596	Na4–O18	2.384(3)	Na5–O25	2.260(4)
				Mean	2.578	Mean	2.507
Na6–O5	2.556(3)	Na7–O8	2.903(3)	Na8–O5	2.473(3)	Na9–O3	2.287(4)
Na6–O8	2.415(3)	Na7–O15	2.979(4)	Na8–O19	2.477(3)	Na9–O4	2.244(4)
Na6–O9	2.506(3)	Na7–O20	2.438(3)	Na8–O22	2.407(3)	Na9–O17	2.444(3)
Na6–O14	2.400(3)	Na7–O21	2.474(3)	Na8–O23	2.842(3)	Na9–O17	2.444(3)
Na6–O16	2.349(3)	Na7–O23	2.351(3)	Na8–O26	2.496(3)	Na9–O26	2.220(4)
Na6–O22	2.519(3)	Na7–O25	2.607(3)	Na8–O29	2.772(3)	Mean	2.328
Mean	2.458	Na7–O29	2.388(3)	Mean	2.578		
		Mean	2.591				
Na10–O2	2.305(4)	Na11–O6	2.488(3)				
Na10–O11	2.312(4)	Na11–O7	2.947(3)				
Na10–O13	2.437(3)	Na11–O17	2.596(3)				
Na10–O13	2.437(3)	Na11–O19	2.527(3)				
Na10–O14	2.313(5)	Na11–O26	2.575(3)				
Mean	2.361	Na11–O27	2.457(3)				
		Na11–O28	2.337(3)				
		Mean	2.561				

replacement of $(PO_4)^{3-}$ by $(HPO_4)^{2-}$ groups, as well as by a replacement of $(OH)^-$ groups by H_2O molecules; the resulting substitution mechanisms are both expressed by the general formula $Na_{4-2x}Fe^{3+}(PO_4)_{2-x}(HPO_4)_x(OH)_{1-x}\bullet xH_2O$.

X-phase

In sample H.283, synthesized at 700 °C from the starting composition $Na_{2.25}Fe^{3+}{}_{2.25}(PO_4)_3$ (Table 1), an unknown phosphate compound was observed as elongated brownish crystals showing a perfect cleavage plane (Fig. 1d). This compound is associated with alluaudite and marićite; its X-ray powder diffraction pattern, as well as the electron-microprobe composition given in Table 5, indicate that it corresponds to "X-phase", a phosphate hydrothermally synthesized by Hatert *et al*. (2006, 2011). The chemical composition of this phase falls in the compositional field of alluaudites, thus indicating that the X-phase certainly corresponds to a high-temperature polymorph of Fe^{2+}-rich alluaudite-type phosphates.

$NaFe^{3+}(P_2O_7)$

The crystal structure of $NaFe^{3+}P_2O_7$ was solved by Gabelica-Robert (1982) in space group $P2_1/c$ [*a* 7.324(1), *b* 7.9045(7), *c* 9.575(2) Å, β 111.86(1)°]; it consists of a heteropolyhedral layered structure in which FeO_6 octahedra and PO_4 tetrahedra form alternating layers. The two layers are connected by corner sharing, and Na atoms occur in elongated cages. In our experiments, $NaFe^{3+}P_2O_7$ was synthesized between 400 and 600 °C, from Fe^{3+}- and Na-rich compositions (Table 1). Electron-microprobe analyses (Table 5) indicate chemical compositions in good agreement with the ideal formula of this diphosphate.

Sodium phosphates

On the Na-rich side of the Na–Fe^{2+}–Fe^{3+} (+PO_4) diagram, sodium phosphates α-, β-, and γ-Na_3PO_4, as well as $Na_2H_2P_2O_7$•$6H_2O$, Na_2HPO_4•nH_2O, NaH_2PO_4•nH_2O, and $Na_2(HPO_4)$•$7H_2O$, were identified by X-ray powder diffraction (Table 1). In polished thin sections, however, these phosphates were frequently dissolved due to the preparation techniques. Electron-microprobe compositions of Na_2HPO_4•nH_2O (Table 5) are in good agreement with the ideal formula of this phosphate.

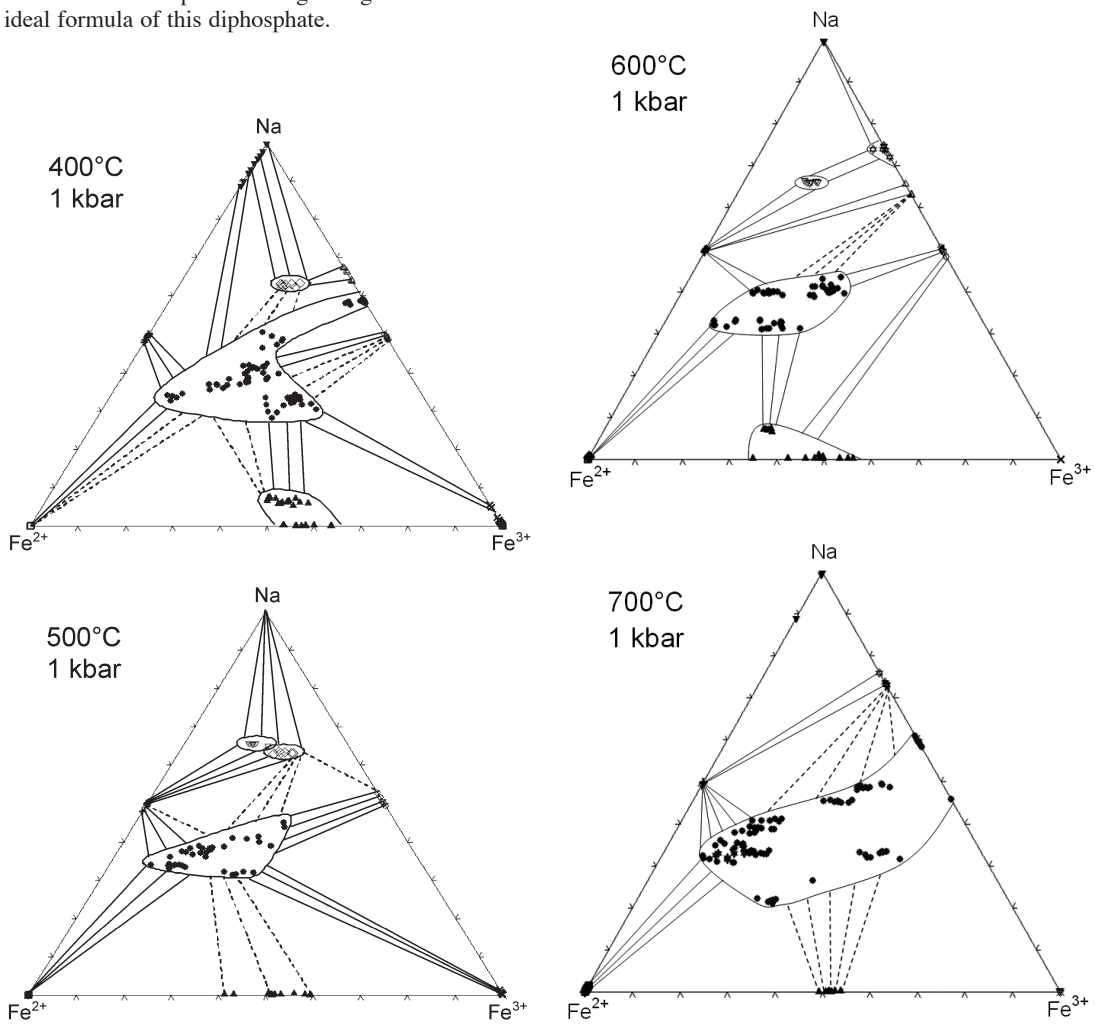

FIG. 5. Diagrams showing the phase relations in the Na–Fe^{2+}–Fe^{3+} (+PO_4) ternary system, at (a) 400 and 500 °C and (b) 600 and 700 °C (*P* = 1 kbar). Dotted lines represent more hypothetical portions of the diagrams. Full circles = alluaudite; empty circles = $NaFe^{3+}(P_2O_7)$; vertical crosses = $NaFe^{2+}(PO_4)$; diagonal crosses = $Fe^{3+}{}_4(PO_4)_3(OH)_3$; full squares = $Fe^{3+}{}_4(P_2O_7)_3$; empty squares = $Fe^{2+}{}_3(PO_4)_2$; full triangles = $Fe^{2+}{}_3Fe^{3+}{}_4(PO_4)_6$; empty triangles = $Na_{4-2x}Fe^{3+}(PO_4)_{2-x}(HPO_4)_x(OH)_{1-x}$•$xH_2O$; full inverse triangles = Na-phosphates; empty inverse triangle = $Na_4Fe^{2+}Fe^{3+}(PO_4)_3$; full stars = X-phase; empty stars = $Na_3Fe^{3+}(PO_4)_2$; empty diamonds = $Na_7Fe^{2+}Fe^{3+}{}_3(PO_4)_6$.

Phase Relations Between 400 and 700 °C

In order to understand the temperature stability of Fe-rich alluaudites, hydrothermal experiments were performed at 400, 500, 600, and 700 °C (1 kbar), starting from several compositions in the Na–Fe^{2+}–Fe^{3+} (+PO_4) ternary system. The results of these experiments (Table 1) are presented graphically in Figure 5, which clearly shows that alluaudites occupy the central portion of the diagram. The alluaudite compositional field covers 12.8, 5.8, 6.0, and 21.1% of the diagram surface, at 400, 500, 600, and 700 °C, respectively. The extremely large compositional field of alluaudites at 700 °C is due to the crystallization of Na-poor or Fe^{3+}-rich samples, with compositions like $Na_{0.94}Fe^{2+}_{2.19}Fe^{3+}_{1.23}(PO_4)_3$ (H.318; Table 3) or $Na_{2.88}Fe^{3+}_{1.97}(PO_4)_{2.78}(HPO_4)_{0.22}$ (H.317; Table 3).

Phosphates observed on the Fe^{3+} pole are $Fe^{3+}_4(PO_4)_3(OH)_3$ and $Fe^{3+}_4(P_2O_7)_3$; the evolution towards Fe^{2+}-rich compositions produces $Fe^{2+}_3Fe^{3+}_4(PO_4)_6$, which is characterized by a large compositional field due to a variable Fe^{2+}/Fe^{3+} ratio and a significant Na content. At the Fe^{2+} pole, sarcopside-type $Fe^{2+}_3(PO_4)_2$ and $Fe^{2+}_2P_2O_7$ occur; evolution towards the Na pole produces marićite, $NaFe^{2+}(PO_4)$, and then the sodium phosphates: α-, β-, and γ-Na_3PO_4, $Na_2H_2P_2O_7$•$6H_2O$, $Na_2(HPO_4)$•$7H_2O$, Na_2HPO_4•nH_2O, and NaH_2PO_4•nH_2O.

Phosphates occurring between the Na and Fe^{3+} poles are different from those described by Lajmi *et al*. (2002) in the Na_3PO_4–$FePO_4$ binary system. According to these authors, three intermediate phosphate compounds exist between Na_3PO_4 and $FePO_4$: $Na_3Fe^{3+}(PO_4)_2$, $Na_3Fe^{3+}_2(PO_4)_3$, and $Na_3Fe^{3+}_3(PO_4)_4$. Starting from the Na pole, the first phosphate compound observed in our experiments is $Na_3Fe^{3+}(PO_4)_2$, which was synthesized at 600 and 700 °C, and shows a structure significantly different from the glaserite-type phosphate compound described by Morozov *et al*. (2001). Then the new phosphate $Na_2Fe^{3+}(HPO_4)(PO_4)\cdot H_2O$ appears, which is described in the present paper for the first time, followed by $Na_3Fe^{3+}_2(PO_4)_3$, which shows an alluaudite structure-type, different from the NASICON structure reported for this composition by Lajmi *et al*. (2002). Finally, $NaFe^{3+}(P_2O_7)$ was synthesized between 400 and 600 °C; at 700 °C, the alluaudite stability field includes all phosphate compounds with Na/(Na + Fe^{3+}) ratios between 0.60 and 0.45 (Fig. 5b).

On the Na-rich side of the diagram, just above the stability field of alluaudites, occur two Na-, Fe^{2+}-, and Fe^{3+}-bearing phosphate compounds: $Na_7Fe^{2+}Fe^{3+}_3(PO_4)_6$, observed at 400 and 500 °C (Fig. 5a), and NASICON-type $Na_4Fe^{2+}Fe^{3+}(PO_4)_3$, observed at 500 and 600 °C (Figs. 5a and b). At 700 °C, these phosphate compounds disappear and are replaced by the assemblage Na_3PO_4 + $NaFe^{2+}PO_4$ + $Na_3Fe^{3+}(PO_4)_2$ (Fig. 5b).

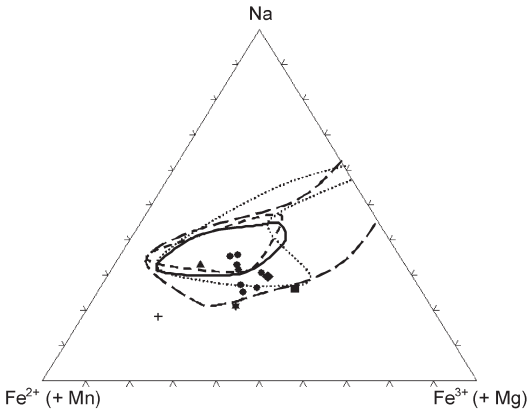

Fig. 6. Compositions of Fe-rich alluaudites, plotted in the Na–Fe^{2+}–Fe^{3+} (+PO_4) ternary diagram. Localities are Angarf-Sud, Morocco (points, Fransolet *et al*. 1985); Hühnerkobel, Bavaria (cross, Mason 1942); Norrö, Norway (triangle, Eriksson 1946); Pleasant Valley Mine, USA (square, Moore & Ito 1979); Tsaobismund, Namibia (diamond, Fransolet *et al*. 1986); La Fregeneda, Spain (star, Roda *et al*. 1996). These compositions are compared with the stability fields of alluaudite-type phosphates, determined in the present study: dotted line = 400 °C; short dashes = 500 °C; solid line = 600 °C; long dashes = 700 °C.

Discussion

Stability of Fe-rich alluaudites

In the present paper, Fe-rich alluaudites were synthesized in the Na–Fe^{2+}–Fe^{3+} (+PO_4) system, at all temperatures between 400 and 700 °C. Alluaudites cover a large stability field in the center of this diagram, thus confirming the existence of primary alluaudites in granitic pegmatites (Fransolet *et al*. 2004, Hatert *et al*. 2006, 2011).

In pegmatites, alluaudite-group minerals generally contain significant amounts of Mn, and Fe-rich compositions are not common. The compositions of these Fe-rich samples, reported in the literature, are plotted in the Na–Fe^{2+}–Fe^{3+} (+PO_4) ternary diagram, and are compared to the alluaudite stability fields determined in the present experimental study (Fig. 6). In order to plot these data, we grouped together Fe^{2+} with Mn, and Fe^{3+} with Mg, since these cations have similar crystal-chemical roles in alluaudite-type phosphates.

Figure 6 clearly shows that the majority of Fe-rich alluaudites fall in the 400 °C stability field, except the sample from Hühnerkobel, Bavaria, which is extremely Ca-rich (Mason 1942), and the sample from La Fregeneda, Spain (Roda *et al*. 1996). Due to their more limited extents, the stability fields determined at 500 and 600 °C do not fit with several natural compositions, thus indicating that these alluaudites certainly crystallized below *ca*. 450 °C. This temperature range is in good agreement with the temperatures determined by Hatert

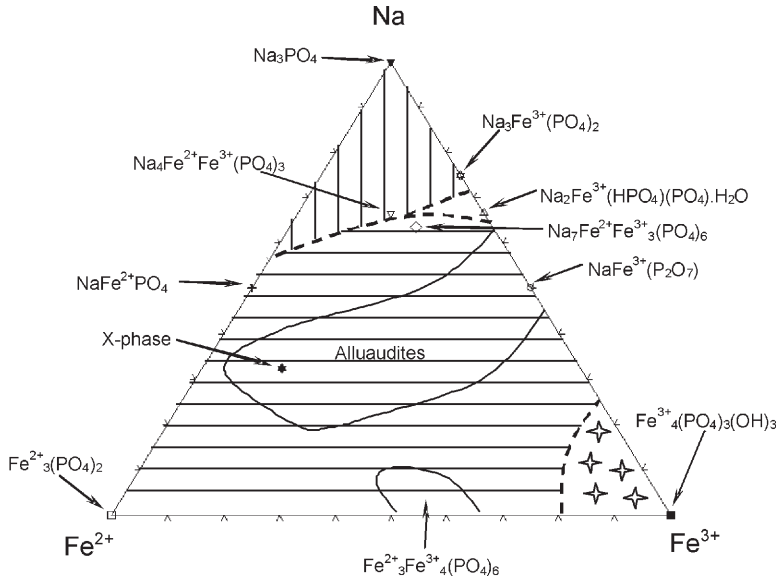

FIG. 7. Structural variations of phosphates synthesized in the Na–Fe^{2+}–Fe^{3+} (+PO_4) ternary system (400–700 °C, 1 kbar). Stars = face-sharing FeO_6 octahedra; horizontal lines = edge-sharing FeO_6 octahedra; white field = corner-sharing FeO_6 octahedra; vertical lines = heteropolyhedral units made up of corner-sharing FeO_6 octahedra and PO_4 tetrahedra.

et al. (2006, 2011) for the crystallization of alluaudites in pegmatites. Moreover, the secondary origin of these samples, produced by Na-metasomatic exchanges from triphylite, ferrisicklerite, or heterosite (Fransolet *et al*. 1985, 1986, Roda *et al*. 1996), obviously confirms the low crystallization temperatures determined in the present study.

The structural complexity of phosphates in the Na–Fe^{2+}–Fe^{3+} (+PO_4) system

As described above, alluaudite-type phosphates are not the only phases which crystallize in the Na–Fe^{2+}–Fe^{3+} (+PO_4) system. A careful examination of the structure types of these phosphates, which are summarized in Table 9, indicates that a correlation exists between the location of the phosphates on the surface of the diagram and their structural complexity.

Considering only the connectivity of the FeO_6 octahedra, we can divide the Na–Fe^{2+}–Fe^{3+} (+PO_4) ternary diagram into four zones (Fig. 7): a first Fe^{3+}-rich zone in which phosphates contain face-sharing octahedra ($Fe^{3+}{}_4(PO_4)_3(OH)_3$), a large zone in which octahedral sites share their edges (sarcopside, alluaudites, marićite,…), a small zone characterized by corner-sharing octahedra ($Na_2Fe^{3+}(HPO_4)(PO_4)\cdot H_2O$), and a last zone in which structures are based on heteropolyhedral units.

The structures located on the Fe-rich sides of the diagram are extremely compact: face-sharing octahedra [$Fe^{3+}{}_4(PO_4)_3(OH)_3$], or edge-sharing octahedra assembled in close-packing (sarcopside). The progressive evolution towards Na-rich compositions implies an increasing "dilution" of FeO_6 octahedra in the structure; these octahedral sites become more and more isolated by large Na atoms. In alluaudites, FeO_6 octahedra share their edges, like in sarcopside, but the structure is less compact since the Na atoms are located in large channels running along the *c* axis. In alluaudites, octahedra form infinite edge-sharing chains, but in $Na_7Fe^{2+}Fe^{3+}{}_3(PO_4)_6$, edge-sharing octahedra are assembled to form tetramers; this indicates that the octahedral clusters become increasingly smaller when evolving towards Na-rich compositions.

Phosphates characterized by heteropolyhedral units (Fig. 7, Table 9) occur on the Na-rich side of the diagram. In the NASICON-type structure of $Na_4Fe^{2+}Fe^{3+}(PO_4)_3$, FeO_6 octahedra share their corners with PO_4 tetrahedra to form an infinite 3D-framework; in the Na-richer phase $Na_3Fe^{3+}(PO_4)_2$, heteropolyhedral double chains occur, thus confirming again the increasing dilution of FeO_6 octahedra in Na-rich phosphates.

TABLE 9. MAIN STRUCTURAL FEATURES OF PHOSPHATES SYNTHESIZED IN THE Na–Fe^{2+}–Fe^{3+} (+PO_4) SYSTEM

Compound	SG	*a*, *b*, *c* (Å)	α, β, γ (°)	V (Å^3)	Structure description	Refs.
$Na_2Fe^{2+}{}_2Fe^{3+}(PO_4)_3$ (alluaudite)	*C*2/*c*	11.849(2) 12.539(1) 6.486(1)	90 114.51(1) 90	876.8(1)	Kinked chains of edge-sharing octahedra, stacked parallel to {101}. Na atoms occur in large channels running along the *c* axis.	1
$Fe^{2+}{}_3(PO_4)_2$ (sarcopside)	*P*2$_1$/*c*	6.026 (8) 4.768(9) 10.44(2)	90 90.0(2) 90	300.0(1)	M1 and M2 octahedra sharing edges. Structure based on close packing of octahedral sites.	2
$NaFe^{2+}(PO_4)$ (maríćite)	*Pmnb*	6.861(1) 8.987(1) 5.045(1)	90 90 90	311.1(1)	Chain of edge-sharing M1 octahedra. M2[10] sites share some faces and edges with M1.	3
$Fe^{3+}{}_4(PO_4)_3(OH)_3$	*C*2/*c*	19.555 (2) 7.376(1) 7.429(1)	90 102.26(1) 90	1047.1(1)	Dimers of face-sharing FeO_6 octahedra, interconnected by sharing corners or via PO_4 tetrahedra.	4
$Fe^{2+}{}_3Fe^{3+}{}_4(PO_4)_6$	$P\bar{1}$	6.361(1) 7.975(1) 9.322(2)	105.27(1) 108.06(1) 101.99(1)	441.6(1)	Chains of edge-sharing Fe1O_6, Fe2O_6, and Fe4O_5 polyhedra. Chains are interconnected by sharing corners with FeO_6 octahedra and PO_4 tetrahedra	5, 6
$Fe^{2+}{}_2(P_2O_7)$	*P*1	5.517(2) 5.255(2) 4.488(1)	98.73(2) 98.33(4) 103.81(2)	122.6(2)	Edge-sharing octahedra forming six-membered rings, the center of which is occupied by a P_2O_7 group.	7
$Fe^{3+}{}_4(P_2O_7)_3$	*P*2$_1$/*n*	7.389(2) 21.337(1) 9.517(2)	90 90(1) 90	1500.4(1)	Fe_2O_9 dimers made of face-sharing octahedra. Dimers form (010) layers connected *via* P_2O_7 groups.	8
$Na_7Fe^{2+}Fe^{3+}{}_3(PO_4)_6$	$R\bar{3}c$	13.392(2) 13.392(2) 17.858(3)	90 90 120	2773.7(8)	Tetramers made of four FeO_6 octahedra sharing edges. Large cavities between the tetramers contain Na atoms.	9
$Na_4Fe^{2+}Fe^{3+}(PO_4)_3$ (nasicon)	$R\bar{3}c$	8.9543(9) 8.9543(9) 21.280(4)	90 90 120	1477.6(4)	Heteropolyhedral framework made of corner-sharing PO_4 tetrahedra and FeO_6 octahedra. Lantern units stacked along *c*, between which occur the 6- and 8-coordinated Na sites.	10
$Na_3Fe^{3+}(PO_4)_2$	$P\bar{1}$	5.3141(6) 8.5853(9) 8.7859(8)	114.429(9) 92.327(9) 106.08(1)	345.1(1)	Heteropolyhedral double chains of corner-sharing PO_4 tetrahedra and FeO_6 octahedra. Chains are interconnected *via* Na cations.	11
$Na_4Fe^{3+}(PO_4)_2(OH)$	*Pnma*	15.5004(8) 7.1465(5) 29.239(2)	90 90 90	3238.9(3)	Chains of corner-sharing FeO_6 octahedra, decorated by PO_4 tetrahedra. NaO_{5-7} polyhedra occur between the chains.	This work
$NaFe^{3+}(P_2O_7)$	*P*2$_1$/*c*	7.324(1) 7.9045(7) 9.575(2)	90 111.86(1) 90	514.5(1)	Heteropolyhedral layered structure, where FeO_6 and PO_4 form alternating layers. Na atoms occur in elongated cages.	12

1. Hatert *et al*. 2005; 2. Moore 1972; Le Page & Donnay 1977; 4. Torardi *et al*. 1989 ; 5. Lightfoot & Cheetham 1989 ; 6. Dal Bo & Hatert 2012 ; 7. Stefanidis & Nord 1982; 8. Elbouaanani *et al*. 2002 ; 9. Lii 1996 ; 10. Hatert 2009 ; 11. Hatert 2007; 12. Gabelica-Robert 1982.

Acknowledgements

This paper is dedicated to André-Mathieu Fransolet, Paul Keller, and François Fontan, for their outstanding contribution to the petrography, mineralogy, and crystal chemistry of pegmatite phosphate minerals. We would like to thank particularly André-Mathieu, who was director of the Laboratory of Mineralogy, University of Liège, for more than 20 years, and incited us to discover the complex but fascinating world of phosphates. Many thanks are due to H.-J. Bernhardt and P. de Parseval, who performed the electron-microprobe analyses at the Ruhr-University of Bochum, Germany, and at the Université Paul Sabatier, Toulouse, France, respectively.

References

Burnham, C.W. (1991) *LCLSQ version 8.4, least-squares refinement of crystallographic lattice parameters*. Departmentt of Earth and Planetary Sciences, Harvard University, 24.

Catti, M. & Franchini-Angela, M. (1976) Hydrogen bonding in the crystalline state. Structure of $Mg_3(NH_4)_2(HPO_4)_4(H_2O)_8$ (hannayite), and crystal-chemical relationships with schertelite and struvite. *Acta Crystallographica* **B32**, 2842–2848.

Černý, P. (1991) Rare-element granitic pegmatites. Part I: Anatomy and internal evolution of pegmatite deposits. *Geosciences Canada* **18(2)**, 49–67.

ČERNÝ, P. & ERCIT, T.S. (2005) The classification of granitic pegmatites revisited. *Canadian Mineralogist* **40**, 2005–2026.

DAL BO, F. & HATERT, F. (2012) $Fe(II)_{2.67}Fe(III)_4(PO_4)_{5.35}(HPO_4)_{0.65}$ and $Fe(II)_{2.23}Fe(III)_4(PO_4)_{4.45}(HPO_4)_{1.55}$, two new mixed-valence iron phosphates. *Acta Crystallographica* **C68,** i83–i85.

ELBOUAANANI, L.K., MALAMAN, B., GÉRARDIN, R., & IJJAALI, M. (2002) Crystal structure refinement and magnetic properties of $Fe_4(P_2O_7)_3$ studied by neutron diffraction and Mössbauer techniques. *Journal of Solid State Chemistry* **163**, 412–420.

ERIKSSON, T. (1946) Triphylin och arrojadit från Norrö muskovit-pegmatit. *Arkiv för Kemi, Mineralogi och Geologi* **23A(8)**, 1–14.

EUGSTER, H.P. (1957) Heterogeneous reactions involving oxidation and reduction at high pressures and temperatures. *Journal of Chemical Physics* **26**, 1760–1761.

FRANSOLET, A.-M. (1975) *Etude minéralogique et pétrologique des phosphates de pegmatites granitiques*. Ph.D. thesis, University of Liège, 333pp.

FRANSOLET, A.-M., ABRAHAM, K., & SPEETJENS, J.-M. (1985) Evolution génétique et signification des associations de phosphates de la pegmatite d'Angarf-Sud, plaine de Tazenakht, Anti-Atlas, Maroc. *Bulletin de Minéralogie* **108**, 551–574.

FRANSOLET, A.-M., KELLER, P., & FONTAN, F. (1986) The phosphate mineral associations of the Tsaobismund pegmatite, Namibia. *Contributions to Mineralogy and Petrology* **92**, 502–517.

FRANSOLET, A.-M., FONTAN, F., KELLER, P., & ANTENUCCI, D. (1998) La série johnsomervilleite-fillowite dans les associations de phosphates de pegmatites granitiques de l'Afrique centrale. *Canadian Mineralogist* **36**, 355–366.

FRANSOLET, A.-M., HATERT, F., & FONTAN, F. (2004) Petrographic evidence for primary hagendorfite in an unusual assemblage of phosphate minerals, Kibingo granitic pegmatite, Rwanda. *Canadian Mineralogist* **42**, 697–704.

GABELICA-ROBERT, M. (1982) The pyrophosphate $NaFeP_2O_7$: A cage structure. *Journal of Solid State Chemistry* **45**, 389–395.

HATERT, F. (2007) Crystal structure of trisodium iron diphosphate, $Na_{2.88}Fe(PO_4)_2$, a synthetic phosphate with hannayite-type heteropolyhedral chains. *Zeitschrift für Kristallographie NCS* **222**, 6–8.

HATERT, F. (2008) The crystal chemistry of the divalent cation in alluaudite-type phosphates: a structural and infrared spectral study of the $Na_{1.5}(Mn_{1-x}M^{2+}_x)_{1.5}Fe_{1.5}(PO_4)_3$ solid solutions (x = 0 to 1, M^{2+} = Cd^{2+}, Zn^{2+}). *Journal of Solid State Chemistry* **181,** 1258–1272.

HATERT, F. (2009) $Na_4Fe^{2+}Fe^{3+}(PO_4)_3$, a new synthetic NASICON-type phosphate. *Acta Crystallographica* **E65**, i30.

HATERT, F., KELLER, P., LISSNER, F., ANTENUCCI, D., & FRANSOLET, A.-M. (2000) First experimental evidence of alluaudite-like phosphates with high Li-content: the $(Na_{1-x}Li_x)MnFe_2(PO_4)_3$ series (x = 0 to 1). *European Journal of Mineralogy* **12**, 847–857.

HATERT, F., HERMANN, R.P., LONG, G.J., FRANSOLET, A.-M., & GRANDJEAN, F. (2003) An X-ray Rietveld, infrared, and Mössbauer spectral study of the $NaMn(Fe_{1-x}In_x)_2(PO_4)_3$ alluaudite-like solid solution. *American Mineralogist* **88**, 211–222.

HATERT, F., REBBOUH, L., HERMANN, R.P., FRANSOLET, A.-M., LONG, G.J., & GRANDJEAN, F. (2005) Crystal chemistry of the hydrothermally synthesized $Na_2(Mn_{1-x}Fe^{2+}_x)_2Fe^{3+}(PO_4)_3$ alluaudite-type solid solution. *American Mineralogist* **90**, 653–662.

HATERT, F., FRANSOLET, A.-M., & MARESCH, W.V. (2006) The stability of primary alluaudites in granitic pegmatites: an experimental investigation of the $Na_2(Mn_{2-2x}Fe_{1+2x})(PO_4)_3$ system. *Contributions to Mineralogy and Petrology* **152**, 399–419.

HATERT, F., OTTOLINI, L., & SCHMID-BEURMANN, P. (2011) Experimental investigation of the alluaudite + triphylite assemblage, and development of the Na-in-triphylite geothermometer: applications to natural pegmatite phosphates. *Contributions to Mineralogy and Petrology* **161**, 531–546.

HATERT, F., RODA-ROBLES, E., DE PARSEVAL, P., & WOUTERS, J. (2012) Zavalíaite, $(Mn^{2+},Fe^{2+},Mg)_3(PO_4)_2$, a new member of the sarcopside group from the La Empleada pegmatite, San Luis Province, Argentina. *Canadian Mineralogist* **50**, 1445–1452.

KAMPF, A.R., STEELE, I.M., & LOOMIS, T.A. (2008) Jahnsite-(NaFeMg), a new mineral from the Tip Top mine, Custer County, South Dakota: Description and crystal structure. *American Mineralogist* **93**, 940–945.

KRIVOVICHEV, S.V., VERGASOVA, L.P., FILATOV, S.K., RYBIN, D.S., BRITVIN, S.N., & ANANIEV, V.V. (2013) Hatertite, $Na_2(Ca,Na)(Fe^{3+},Cu)_2(AsO_4)_3$, a new alluaudite-group mineral from Tolbachik fumaroles, Kamchatka peninsula, Russia. *European Journal of Mineralogy* **25**, 683–691.

LAJMI, B., HIDOURI, M., RZEIGUI, M., & BEN AMARA, M. (2002) Reinvestigation of the binary diagram Na_3PO_4-$FePO_4$ and crystal structure of a new iron phosphate $Na_3Fe_3(PO_4)_4$. *Materials Research Bulletin* **37**, 2407–2416.

LE PAGE, Y. & DONNAY, G. (1977) The crystal structure of the new mineral maricite, $NaFePO_4$. *Canadian Mineralogist* **15**, 518–521.

LIGHTFOOT, P. & CHEETHAM, A.K. (1989) Neutron diffraction study of the cation distributions in the systems $Fe_{7-x}M_x(PO_4)_6$ (M = Mn or Co). *Journal of the Chemical Society, Dalton Transactions* **9**, 1765–1769.

Lii, K.-H. (1996) $Na_7Fe_4(PO_4)_6$: a mixed-valence iron phosphate containing a tetramer of edge-sharing FeO_6 octahedra. *Journal of the Chemical Society, Dalton Transactions* **6**, 819–822.

Mason, B. (1941) Minerals of the Varuträsk pegmatite. XXIII. Some iron-manganese phosphate minerals and their alteration products, with special reference to material from Varuträsk. *Geologiska Föreningen i Stockholm Förhandlingar* **63**, 117–175.

Mason, B. (1942) Some iron manganese phosphate minerals from the pegmatite at Hühnerkobel in Bavaria. *Geologiska Föreningen i Stockholm Förhandlingar* **64**, 335–340.

Maximov, B., Bolotina, N., & Tamazyan, R. (1994) Structural phase transitions in the superionic conductors $Na_9\{Fe_2[PO_4]_4(O,F)_2\}$ and $Na_8\{Ti_2[PO_4]_4O_2\}$ in the temperature range 520–540 K. *Zeitschrift für Kristallographie* **209**, 649–656.

Moore, P.B. (1972) Sarcopside: its atomic arrangement. *American Mineralogist* **57**, 24–35.

Moore, P.B. & Ito, J. (1979) Alluaudites, wyllieites, arrojadites: crystal chemistry and nomenclature. *Mineralogical Magazine* **43**, 227–235.

Morozov, V.A., Lazoryak, B.I., Malakho, A.P., Pokholok, K.V., Polyakov, S.N., & Terekhina, T.P. (2001) The glaserite-like structure of double sodium and iron phosphate $Na_3Fe(PO_4)_2$. *Journal of Solid State Chemistry* **160**, 377–381.

Norton, F.J. (1955) Dissociation pressures of iron and copper oxides. *General Electric Research Laboratory Report* **55-R1-1248**.

Oxford Diffraction (2007) *CrysAlis CCD and CrysAlis RED, version 1.71*. Oxford Diffraction, Oxford, England.

Quensel, P. (1957) The paragenesis of the Varuträsk pegmatite, including a review of its mineral assemblage. *Arkiv för Mineralogi och Geologi* **2(2)**, 9–125.

Redhammer, G.J., Roth, G., Tippelt, G., Bernroider, M., Lottermoser, W., & Amthauer, G. (2004) The mixed-valence iron compound $Na_{0.1}Fe_7(PO_4)_6$: crystal structure and ^{57}Fe Mössbauer spectroscopy between 80 and 295 K. *Journal of Solid State Chemistry* **177**, 1607–1618.

Roda, E., Fontan, F., Pesquera, A., & Velasco, F. (1996) The phosphate mineral association of the granitic pegmatites of the Fregeneda area (Salamanca, Spain). *Mineralogical Magazine* **60**, 767–778.

Rondeux, M. & Hatert, F. (2010) An X-ray Rietveld and infrared spectral study of the $Na_2(Mn_{1-x}M^{2+}_x)Fe^{2+}Fe^{3+}(PO_4)_3$ (x = 0 to 1, M^{2+} = Mg, Cd) alluaudite-type solid solutions. *American Mineralogist* **95**, 844–852.

Schmid-Beurmann, P. (2000) Synthesis and phase characterization of a solid solution series between β-$Fe_2(PO_4)O$ and $Fe_4(PO_4)_3(OH)_3$. *Journal of Solid State Chemistry* **153**, 237–247.

Schmid-Beurmann, P, (2001) Stability properties and phase relations of $Fe^{3+}_{4-x}Fe^{2+}_{3x}(PO_4)_3(OH)_{3-3x}O_{3x}$ in the quaternary system FeO-Fe_2O_3-P_2O_5-H_2O. *Journal of Materials Chemistry* **11**, 660–667.

Sheldrick, G.M. (2008) A short history of SHELX. *Acta Crystallographica* **A64**, 112–122.

Simmons, W.B., Webber, K.L., Falster, A.U., & Nizamoff, J.W. (2003) *Pegmatology: Pegmatite Mineralogy, Petrology & Petrogenesis*. Rubellite Press, New Orleans, Louisiana, United States (176).

Stefanidis, T. & Nord, A.G. (1982) The crystal structure of iron(II) diphosphate, $Fe_2P_2O_7$. *Zeitschrift für Kristallographie* **159**, 255–264.

Torardi, C.C., Reiff, W.M., & Takacs, L. (1989) Synthesis, crystal structure, and magnetism of $Fe_4(OH)_3(PO_4)_3$ and $V_4O(OH)_2(PO_4)_3$: Chains of M_2O_9 dimers connected by hydroxyl groups. *Journal of Solid State Chemistry* **82**, 203–215.

Tuttle, O.F. (1949) Two pressure vessels for silicate-water studies. *Geologicla Society of America Bulletin* **60**, 1727–1729.

Vignola, P., Hatert, F., Fransolet, A.-M., Medenbach, O., Diella, V., & Andò, S. (2013) Karenwebberite, $Na(Fe^{2+},Mn^{2+})PO_4$, a new member of the triphylite group from the Malpensata pegmatite, Lecco province, Italy. *American Mineralogist* **98**, 767–772.

Wilson, A.J.C. (1992) *International Tables for X-ray Crystallography, Volume C*. Kluwer Academic Press, London, 883pp.

Received March 26, 2014. Revised manuscript accepted April 4, 2014.